nature communications

Article

https://doi.org/10.1038/s41467-025-60463-4

# TIM3-blockade synergizes with IL2 in alleviating intra-tumoral CD8$^+$T cell exhaustion

Received: 12 July 2024

Accepted: 23 May 2025

Published online: 03 June 2025

Check for updates

Xuhao Zhang[1,2,5] ✉, Yu Gao[1,5], Huiping Liao[3,5], Wenyan Wang[1], Zaili Yang[1], Weian Cao[1], Ge Li[4], Jing Wen[1], Gencheng Han[4] & Yang-Xin Fu[1,3] ✉

TIM3, a T-cell inhibitory receptor, is expressed on exhausted T cells in the TME. Progressive loss of IL2-secretion is an early sign of diminished effector function in TILs, which raises the possibility of IL2 loss driving exhaustion of TILs. We show that endogenous IL-2 is required for the antitumor effect of anti-TIM3. Selective delivery of IL-2 to TIM3$^{high}$ TILs via an engineered anti-TIM3-Pro-IL2 fusion enhances anti-TIM3 efficacy, while reducing IL2 toxicity. IL2 activity is inhibited at the acidic pH of the TME, thus an IL2 mutein (IL2V2) with sustained activity at low pH is integrated into the construct. Mechanistically, TIM3-ProIL2V2 not only reactivates TIM3$^+$ TILs but also facilitates the activation and expansion of TIM3$^-$ TILs, which in turn provide a sustained source of effector T cells. TIM3-ProIL2V2 is efficient in multiple tumor models, including tumors in humanized mice. TIM3-ProIL2V2 has the potential to overcome anti-PD-1/L1 resistance in cold cancers.

In the intricate battlefield of tumor microenvironment (TME), tumors ingeniously develop an array of strategies to dampen the body's immune defense, allowing them to proliferate while evade immune detection[1]. These strategies include the upregulation of immune checkpoints that leads to the exhaustion of tumor-infiltrating lymphocytes (TILs)[2], a scarcity of critical cytokines like IL-2 and IFN-γ[1], and an acidic shift in the TME that hampers the effectiveness of cytokines and antibodies[3]. T cell immunoglobulin and mucin domain-containing protein 3 (TIM3) is a poorly defined immune checkpoint molecule closely linked to exhausted T cells and myeloid cells[4]. TIM3 is highly expressed inside TME which raise possible target for anti PD-1 resistant patients[5].

Cytokines are essential regulators of T cell maturation, activation, and survival, shaping their function and fate. However, it is unclear if and which cytokines can rejuvenate exhausted T cells, to produce effector molecules for anti-tumor immunity[6,7]. Throughout the progression of exhausted TILs, CD8$^+$ T cells undergo a hierarchical loss of effector functions, beginning with the reduced IL-2 production and limited proliferative capacity, followed by subsequent reduced production of other cytokines like IFN-γ, thus suggesting that IL-2 deficiency might drive the terminal exhaustion in TILs[6,8]. Building on these observations, we hypothesize that reinstating IL-2 signaling may be essential for the full rejuvenation of these exhausted T cells or limiting the exhaustion. Recent findings highlight potential of IL-2 in sustaining a pool of PD-1$^+$TCF-1$^+$ stem-like CD8$^+$ T cells within tumors, crucial for ongoing immune response[9]. Expansion and differentiation of tumor specific stem-like TILs into effector TILs exert crucial roles for tumor immunotherapies based on IL-2 therapy[10,11]. IL-2 is also commonly used to boost T-cell function and number in T-cell therapy[12,13]. However, IL-2's clinical application faces obstacles, including its rapid systemic clearance, significant toxic side effects, and a propensity to expand Tregs over CD8$^+$ T cells[14], coupled with its diminished activity in the acidic TME[15].

To address these hurdles, we firstly generate mutein IL-2 (IL2V2) that become low pH resistance to keep activity of IL-2 in the acidic TME, which also has higher affinity to IL2Rβ to increase the binding to effector cells over Tregs[3,16]. To mitigate its toxicity, we engineer a cytokine receptor-based IL-2V2 prodrug (ProIL2V2) that combines IL-

[1]Department of Basic Medical Sciences, School of Medicine, Tsinghua University, Beijing, China. [2]Tsinghua-Peking Center for Life Sciences, Tsinghua University, Beijing, China. [3]Changping Laboratory, Beijing, China. [4]Beijing Institute of Basic Medical Sciences, Beijing, China. [5]These authors contributed equally: Xuhao Zhang, Yu Gao, Huiping Liao. ✉e-mail: xuhaozhang@tsinghua.edu.cn; yangxinfu@tsinghua.edu.cn

2V2 with an IL-2Rα, linked by a matrix metalloproteinase (MMP) substrate to prevent IL-2V2 from binding its receptor in peripheral tissues. MMPs, which are highly expressed in various tumor types and play a role in tumor angiogenesis and invasion[17,18], can cleave ProIL2V2, thereby releasing IL-2 specifically within the TME. ProIL2V2 is tumor-activating IL-2 and cannot effectively activate NK or T cells in periphery to limit its toxicity. Given TIM3's prevalent expression on the TIL inside the TME leading to their dysfunction, it raises a prime target for the targeted delivery of ProIL2V2 into those dysfunctional T cells using anti-TIM3 antibodies, which releases the inhibition of exhausted T cells, and also brings IL2V2 to exert synergistic action to rejuvenate the exhausted T cells.

We engineer and fuse such ProIL2V2 into C-terminal of anti-TIM3-Fc as TIM3-ProIL2V2. We then explore if and how TIM3-ProIL2V2 could preferentially target IL-2 on TME to rejuvenate different subset of TILs for enhancing antitumor efficacy with minimal toxicity. Anti-TIM3 antibodies can directly deliver sufficient amount of IL-2 to dysfunctional T cells within TME, even in tumors lacking specific or well-characterized antigens. Therefore, TIM3-ProIL2V2 is likely to be a more versatile anti-tumor drug.

## Results

### IL2V2 paired with anti-TIM3 synergistically amplifies the antitumor effect

Tumor reactive T cells within the TME often become exhausted after prolonged exposure to tumor antigens, characterized by a lack of proliferation and diminished effector functions[19]. Our analysis, supported by RNA sequencing data from survival analysis via the KM plotter for advanced colorectal adenocarcinoma and breast cancer, revealed a negative correlation between high TIM3 levels, low IL-2 expression, and poor clinical outcomes (Supplementary Fig. 1A, B)[20]. To further understand the role of TIM3, we examined its expression in the MC38, a mouse colon cancer model, finding significantly higher levels of TIM3 on $CD8^+$ T cells within the established tumor, compared to those in the spleen and peripheral blood in advanced cancer (Fig. 1A). Anti-TIM3 antibodies were found to only partially delay $CD8^+$ T cell exhaustion, enhanced antitumor immunity and slowed tumor growth at early stage (Fig. 1B)[5,21]. To test if endogenous IL-2 is required for anti-TIM3 mediated tumor control, we blocked IL-2 during anti-TIM3 treatment. Indeed, the effectiveness of anti-TIM3 appeared to be contingent upon the IL-2 signaling pathway, as blocking IL-2 signaling negated the benefits of anti-TIM3 treatment (Fig. 1B). When tumor became advanced, IL-2 signaling pathways became weaken[22,23]. We hypothesized that high expression of TIM3 and limited IL-2 in TME facilitate immune evasion. Given the limited impact of anti-TIM3 and IL-2 monotherapies on advanced tumors, we explored a combination therapy approach. Remarkably, intraperitoneal administration of both anti-TIM3 and IL-2 demonstrated significant therapeutic benefits (Supplementary Fig. 1C). But the high therapeutic dose of combination therapy still failed to eradicate the advanced tumor. New strategies to target IL-2 to dysfunctional TILs might be a better way to restore T cell function without systemic toxicity.

Advanced tumors have low pH TME while IL-2 is sensitive to low pH with lower activities. Therefore, we first need to develop low pH resistant mutated IL-2. Using yeast display technique, we developed a pH-selective IL2V2 through mutational selection which demonstrated even higher affinity to IL-2Rβ in the acidic condition than wild-type (WT) IL-2 in the neutral environment (Fig. 1C).

Given TIM3's prevalent expression on the TIL and badly needed IL-2 for TILs inside the TME, we wondered if anti-TIM3 preferentially bring functional IL-2 $TIM3^+$ TILs. IL2V2 was then fused into C-terminal of anti-TIM3 antibody, called TIM3-IL2V2 (Fig. 1D). This design aimed to enhance tumor targeting for accurate delivery of IL-2 to TME, in order to reduce peripheral consumption and toxicity in the meanwhile. In the MC38 tumor model, TIM3-IL2V2 outperformed other treatments, showcasing superior antitumor efficacy (Fig. 1E). However, it was important to note that despite its effectiveness, TIM3-IL2V2 was associated with significant peripheral toxicity, as evidenced by weight loss in treated mice (Fig. 1F). This finding underscores the need for further refinement in the therapeutic strategy to balance efficacy with safety.

### TIM3-ProIL2V2 generates strong antitumor efficacy with reducing toxicity

To mitigate IL-2 toxicity, we designed a series of TIM3-targeted proIL2V2 fusion proteins aimed at modulating the affinity and activity of IL2V2 on various type of TILs. We constructed five distinct fusion proteins: TIM3-IL2V2-MMPs-Rα, TIM3-IL2V2-Rα, TIM3-Rα-IL2V2, TIM3-Rα-MMPs-IL2V2, TIM3-Rα-MMPs-IL2 (Fig. 2A). Since tumor cells or inflammatory cells express higher level of MMPs to allow tumor to invade into normal tissues nearby[17,18], we engineered TIM3-IL2V2-MMPs-Rα to allow Rα to be removed inside TME as linker between IL2 and Rα is MMP14 sensitive sequences. In this case, the fusion protein TIM3-IL2V2-MMPs-Rα releases the activity of IL2V2 and remains to target $TIM3^+$ TILs through cis-delivery. To determine if IL-2V2 needs to be remained with TIM3 positive cells, we also prepared TIM3-Rα-MMPs-IL2V2 to allow IL2V2 to release from TIM3 antibody as negative control. To determine whether IL-2V2 release by MMP cleavage within the TME is important for treatment, we generated two construct variants: TIM3-IL2V2-Rα and TIM3-Rα-IL2V2, which lack MMP-sensitive linkers, and compared them to TIM3-IL2V2-MMPs-Rα and TIM3-Rα-MMPs-IL2V2. We first tested the ability of these constructs to block IL-2V2 activity with Rα and evaluated the restoration of activity upon MMP cleavage by assessing T cell proliferation using the murine T cell line CTLL2 in vitro (Supplementary Fig. 2A). TIM3-IL2V2-Rα exhibited approximately 60-fold reduced activity (as measured by IC50) compared to TIM3-IL2V2 when tested for IL-2 activity using WT CTLL-2 cells, which lack TIM3 expression. Other constructs with IL-2R, such as TIM3-ProIL2V2, also showed reduced IL-2 activity in WT CTLL-2 cells. However, this activity was fully restored upon MMP cleavage (Supplementary Fig. 2A). In contrast, when tested on TIM3-positive CTLL-2 cells, constructs such as TIM3-ProIL2V2, TIM3-Rα-IL2V2, TIM3-IL2V2-MMP-Rα, and TIM3-IL2V2-Rα regained IL-2 activity comparable to TIM3-IL2V2 (Supplementary Fig. 2B). These results confirm that TIM3-ProIL2V2 and TIM3-IL2V2-Rα efficiently deliver IL-2 to TIM3-positive T cells, even when IL-2's binding affinity is reduced by receptor blockade, ultimately leading to fully restored IL-2 activity. The comparable bioactivity observed between TIM3-IL2V2 and IL-2-blocked constructs, such as TIM3-ProIL2V2, TIM3-Rα-IL2V2, TIM3-IL2V2-MMP-Rα, and TIM3-IL2V2-Rα, in TIM3-positive CTLL2 cells can be attributed to the cis delivery of IL-2 to TIM3-positive T cells, mediated by the anti-TIM3 component.

Cis-delivery of low affinity IL-2 to $PD\text{-}1^+$ cells has been shown to be potent[10,22,24]. We hypothesized that TIM3-IL2V2-MMPs-Rα would be the most potent among 4 groups, because the concealed IL2V2 part was delivered to IL-2 receptors in cis via binding to the $TIM3^+$ TILs, and then the activity of IL2V2 was restored after MMPs digestion inside TME. Our experiments in mice bearing established MC38 tumors treated intraperitoneally with these fusion proteins, yielded surprising results. Among the variants, TIM3-Rα-MMPs-IL2V2, referred to as TIM3-ProIL2V2, unexpectedly emerged as the most effective protein among all four groups with reduced side effects, even at low doses (Fig. 2B, C), indicating release of IL2V2 is required. In head-to-head comparisons against TIM3-ProIL2 (TIM3-Rα-MMPs-IL2) in the same tumor model, TIM3-ProIL2V2 (TIM3-Rα-MMPs-IL2V2) demonstrated superior antitumor immunity, whereas an equivalent dose of combination treatment of claudin-ProIL2V2 (isotype control of TIM3-ProIL2V2) and anti-TIM3 had almost no effect at all, underscoring the indispensable role of TIM3 targeting and the enhanced potency of the IL2V2 variant (Fig. 2D, E). Furthermore, we evaluated the potential of TIM3-ProIL2V2

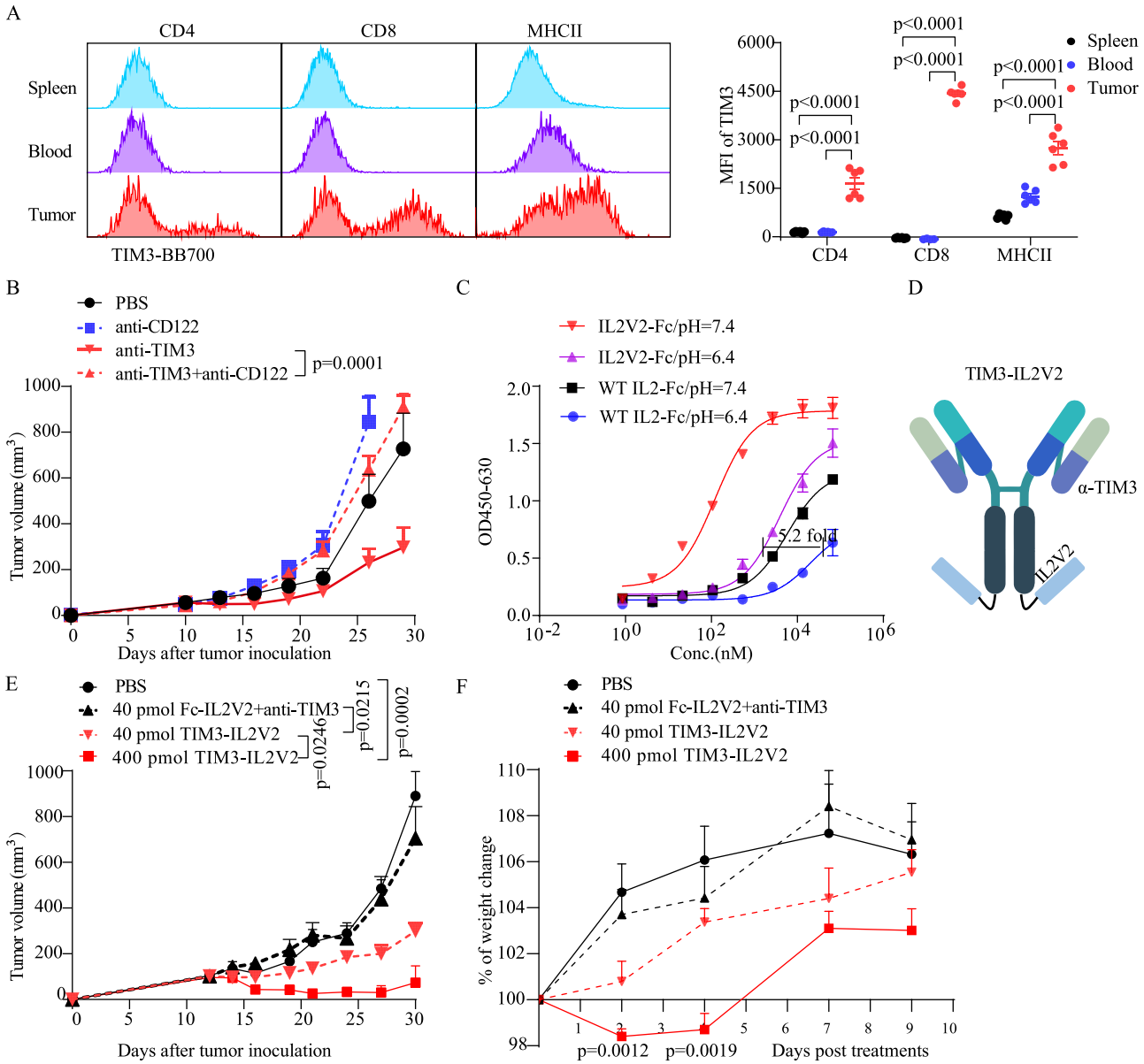


**Fig. 1 | IL-2 paired with anti-TIM3 synergistically amplifies the antitumor effect.** **A** Spleens, PBMCs and tumor tissues were collected from MC38 tumor-bearing mice (female C57BL/6 mice) 14 days post-inoculation. Cells were isolated and stained for flow cytometric analysis. TIM3 expression was analyzed on $CD4^+$, $CD8^+$, and $MHC\text{-}II^+$ cells in spleen, peripheral blood, and tumor samples from MC38 tumor-bearing mice ($n = 6$/group). **B** Female C57BL/6 mice ($n = 6$/group) were inoculated with $5 \times 10^5$ MC38 tumor cells and treated i.p. with 200 μg anti-TIM3 and/or 200 μg anti-IL-2Rβ on day 9. Tumor volume was measured as indicated. **C** 100 ng IL-2 Rβ protein was used to coat the plates, and the binding of biotin-labeled IL2V2-Fc or WT IL2-Fc was detected by Elisa at different pH levels of serial dilutions ($n = 3$/group). **D** Schematic diagram of TIM3-IL2V2. **E**, **F** Female C57BL/6 mice ($n = 5$/group) were inoculated with $5 \times 10^5$ MC38 tumor cells and were treated i.p. with indicated doses of TIM3-IL2V2: 40 or 400 pmol (8 μg or 80 μg), or 40 pmol IL2V2-Fc (5 μg) combined with 40 pmol anti-TIM3 (6 μg). Tumor volumes (**E**) and Body weights (**F**) were measured as indicated. Data are shown as mean ± SEM and representative of two to three independent experiments. *P* value was determined by unpaired two-tailed *t* tests (**A**–**C**, **E**, **F**).

to induce a durable immune response. Mice cured of their tumors were rechallenged with a higher dose of the same tumor cells, and remarkably, all mice successfully rejected the reintroduced tumors (Fig. 2F), indicating the establishment of a protective memory response.

To assess the safety profile of TIM3-ProIL2V2, we examined the serum levels of IFN-γ in mice treated with varying doses of TIM3-IL2V2, TIM3-ProIL2, and TIM3-ProIL2V2. The significantly lower IFN-γ levels in TIM3-ProIL2V2 and TIM3-ProIL2-treated mice, compared to those treated with TIM3-IL2V2, suggested a safer profile for TIM3-ProIL2V2 (Fig. 2G). We explored the tumor-targeting efficacy of TIM3-ProIL2V2 through biodistribution studies, revealing significantly higher tumor accumulation of TIM3-ProIL2V2 compared to a control fusion protein, highlighting the critical role of the anti-TIM3 component in TME targeting (Supplementary Fig. 2C). This mechanism of TME targeting likely contributes to the selective tumor-targeted action and pro-form of TIM3-ProIL2V2, enhancing its therapeutic efficacy while reducing systemic toxicity.

## Pre-existing $TIM3^+CD8^+$TILs are the targets of anti-TIM3-ProIL2V2

In our investigation into the cellular mechanisms underlying the efficacy of TIM3-ProIL2V2, we explored the role of various immune cells since IL-2 could target on NK cells. We initiated our study using *Rag1*$^{-/-}$

https://doi.org/10.1038/s41467-025-60463-4

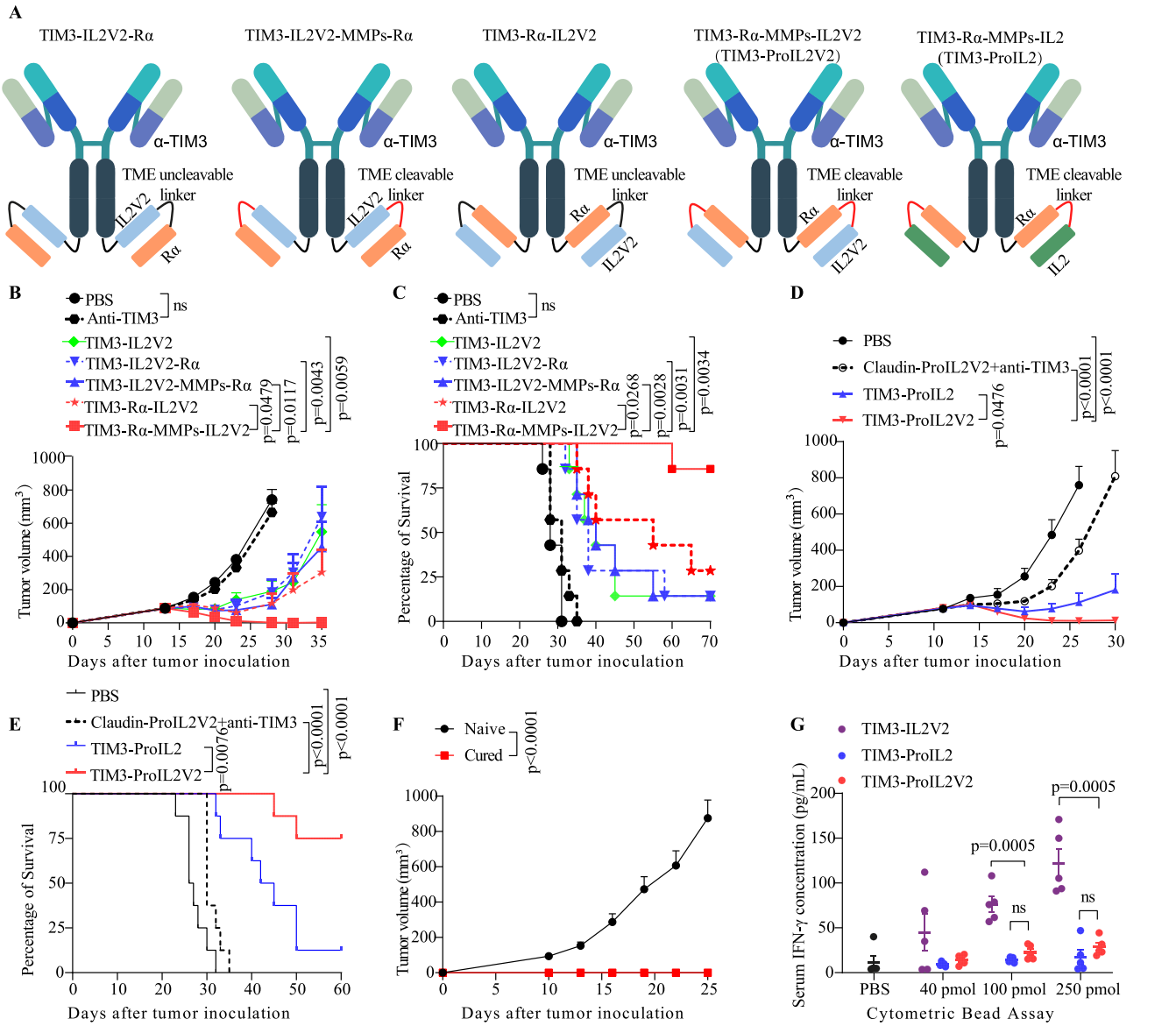


**Fig. 2 | TIM3-ProIL2V2 generates strong antitumor efficacy with reducing toxicity. A** Schematic diagram of TIM3-targeting-ProIL2V2 and TIM3-ProIL2. **B**, **C** MC38 tumor-bearing female mice ($n = 7$/group) were i.p. treated with with equal molar amounts (40 pmol) of anti-TIM3 (6 μg), TIM3-IL2V2-MMPs-Rα (10 μg), TIM3-IL2V2-Rα (10 μg), TIM3-Rα-MMPs-IL2V2 (10 μg), TIM3-Rα-MMPs-IL2V2 (10 μg) and TIM3-IL2V2 (8 μg) on day 14 and 17 post inoculation. Tumor volume (**B**) was measured as indicated and the corresponding mouse survival curve was shown in (**C**). **D**, **E** Female MC38 tumor-bearing mice ($n = 8$/group) were i.p. treated with with equal molar amounts (40 pmol) of TIM3-ProIL2V2 (TIM3-Rα-MMPs-IL2V2, 10 μg) and TIM3-ProIL2 (TIM3-Rα-MMPs-IL2, 10 μg) on day 14 and 17 post inoculation. Tumor volume (**D**) was measured as indicated and the mouse survival curve was shown in (**E**). **F** MC38 bearing female C57BL/6 mice ($n = 6$/group) were treated with TIM3-ProIL2V2 on day 14 and 17 after tumor inoculation. Cured mice were rechallenged with $2 \times 10^6$ MC38 tumor cells 30 days post treatment. **G** Serum IFN-γ levels were measured by cytometric bead assay. Female C57BL/6 mice bearing MC38 tumors ($n = 5$ per group) were i.p. treated with indicated doses of TIM3-IL2V2, TIM3-ProIL2V2 or TIM3-ProIL2: 40 pmol, 100 pmol and 250 pmol on day 14 after tumor inoculation. Serum samples was collected 24 h after the first injection. Data are shown as mean ± SEM and representative of two to three independent experiments. *P* value was determined by unpaired two-tailed *t* tests (**B**, **D**, **F**, **G**). Statistical analyses of survival curve were compared using a log-rank test (**C**, **E**).

mice, which lack adaptive immunity but more NK activity. We observed that the antitumor effects of TIM3-ProIL2V2 were completely nullified in these mice, underscoring the indispensable role of adaptive immunity in the therapeutic process (Fig. 3A). To further dissect the contributions of specific immune cell types, we conducted depletion experiments using anti-NK1.1 antibodies to target NK cells and anti-CSF1R antibodies to target macrophages in WT mice, neither of which impacted the effectiveness of TIM3-ProIL2V2[25]. This finding suggested that these cell types were not critical mediators of the antitumor action (Fig. 3B). Subsequent depletion of T-cell subsets with anti-CD4 or anti-CD8 antibodies revealed that the presence of $CD8^+$ T cells, rather than $CD4^+$ T cells, was crucial for the therapeutic outcome (Fig. 3C). To study if continuing influx of T cells or preexisting T cells are required for the efficacy of TIM3-ProIL2V2, we use FTY720, a compound that prevents T cells from leaving lymph nodes and diminishes T cells in the blood, thus no new flux of T cells into tumor during treatment[26]. Additional FTY720 one day before TIM3-ProIL2V2 treatment did not hinder the therapy's success (Fig. 3D), indicating that preexisting T cells within the TME were sufficient to control tumor.

TIM3 is expressed on not only T cells but also on myeloid cells[27,28]. To clarify the role of TIM3 expression in various immune cell populations within the TME, we utilized conditional knockout mice with TIM3 specifically deleted in dendritic cells ($Zbtb46^{Cre}$ $Havcr2^{fl/fl}$), macrophages ($Lyz2^{Cre}$ $Havcr2^{fl/fl}$), and T cells ($Cd4^{Cre}$ $Havcr2^{fl/fl}$). The

https://doi.org/10.1038/s41467-025-60463-4

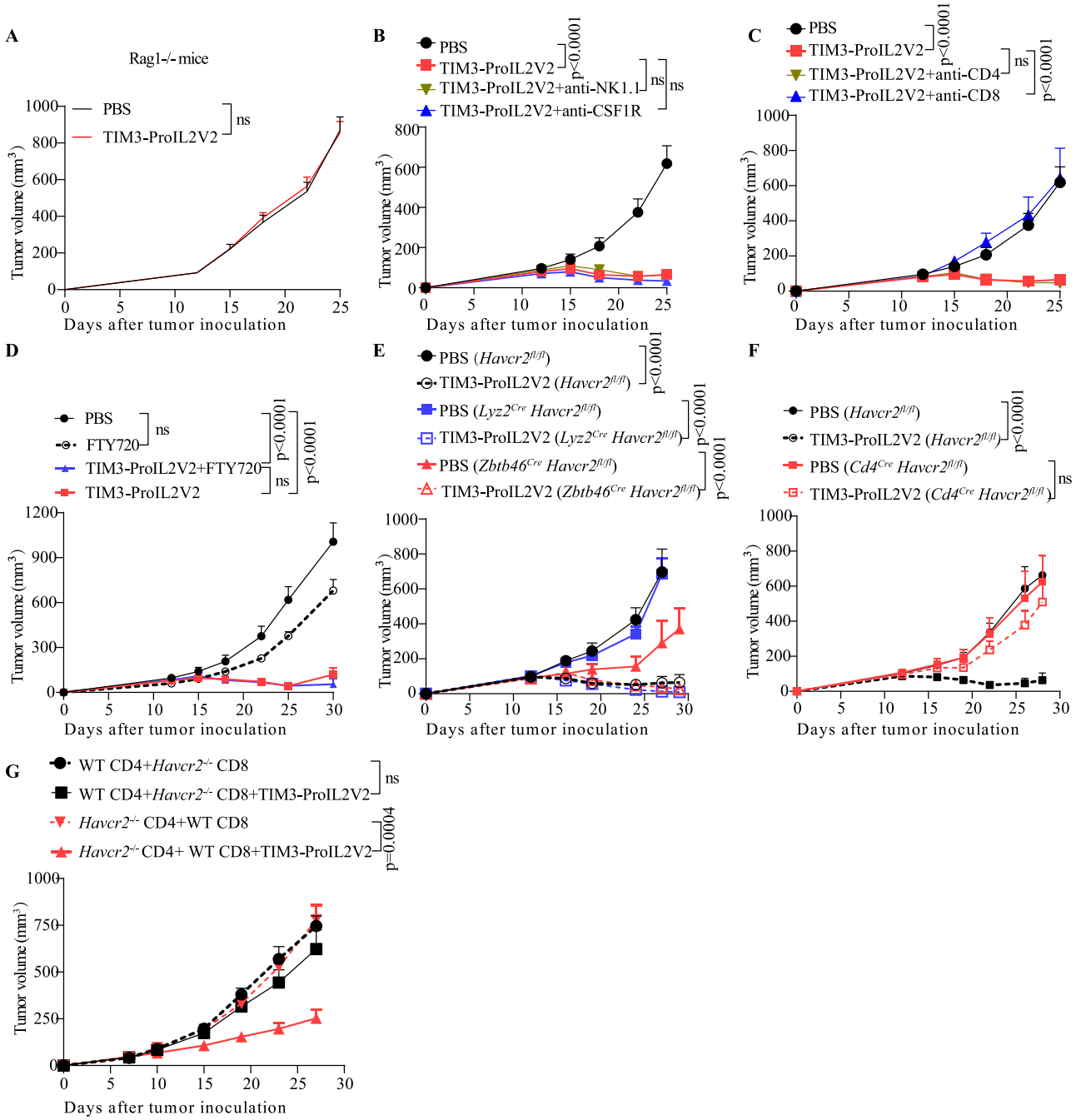


**Fig. 3 | Pre-existing CD8 T cells and TIM3 on CD8⁺T cells is essential for the antitumour effect of TIM3-ProIL2V2. A** Female *Rag1* $^{-/-}$ mice ($n = 5$/group) were inoculated with $5 \times 10^5$ MC38 cells and i.p. treated with 10 μg TIM3-ProIL2V2 on day 12 and 15 after tumor innoculation. Tumor volume was measured as indicated. **B** Female C57BL/6 mice ($n = 6$/group) were inoculated with $5 \times 10^5$ MC38 cells and i.p. treated with 10 μg TIM3-ProIL2V2 on day 14 and 17. For cell specific depletion, 500 μg anti-CSF1R or 200 μg anti-NK1.1 was administrated one day before treatment initiation and then twice a week for 2 weeks. **C** Female C57BL/6 mice ($n = 6$/group) were inoculated with $5 \times 10^5$ MC38 cells and i.p. treated with 10 μg TIM3-ProIL2V2 twice on day 14 and 17. For cell specific depletion, 200 μg anti-CD4 or anti-CD8 was administrated one day before treatment initiation and then twice a week for 2 weeks. **D** Female C57BL/6 mice ($n = 6$/group) were inoculated with $5 \times 10^5$ MC38 cells and i.p. treated with 10 μg TIM3-ProIL2V2 on day 14 and 17. FTY720 was administrated at 20 μg one day before treatment initiation and then every other day for 2 weeks. **E** Female *Havcr2*$^{fl/fl}$ mice, *Zbtb46-Cre Havcr2*$^{fl/fl}$ mice or *Lyz2-Cre Havcr2*$^{fl/fl}$ mice ($n = 6$/group) were inoculated with $5 \times 10^5$ MC38 tumor cells and i.p. treated with 10 μg TIM3-ProIL2V2 on day 14 and 17 after tumor inoculation. **F** Female *Havcr2*$^{fl/fl}$ mice or *Cd4-Cre Havcr2*$^{fl/fl}$ mice ($n = 6$/group) were inoculated with $5 \times 10^5$ MC38 tumor cells and i.p. treated with 10 μg TIM3-ProIL2V2 on day 14 and 17 after tumor inoculation. **G** MC38 tumor-bearing female *Rag1*$^{-/-}$ mice ($n = 5$/group) were transferred $1.5 \times 10^6$ *Havcr3*$^{-/-}$ CD4⁺T cells plus $1.5 \times 10^6$ WT CD8⁺T cells or $1.5 \times 10^6$ WT CD4⁺T cells plus $1.5 \times 10^6$ *Havcr3*$^{-/-}$ CD8⁺T cells 2 days after tumor inoculation. 10 μg TIM3-ProIL2V2 was administrated on day 10 and 13 after tumor inoculation. Data are shown as mean ± SEM and representative of two to three independent experiments. *P* value was determined by unpaired two-tailed *t* tests (**A**–**D**, **E**–**G**).

therapeutic efficacy of TIM3-ProIL2V2 remained intact in mice lacking TIM3 on dendritic cells and macrophages but was lost in mice with T-cell-specific TIM3 knockout (Fig. 3E, F), highlighting the critical role of TIM3 on T cells but not myeloid cells for the success of the treatment. To elucidate which T cell subsets are important for the treatment, we transferred *Havcr3*$^{-/-}$ CD4⁺ T cells plus WT CD8⁺ T cells or WT CD4⁺ T cells plus *Havcr3*$^{-/-}$ CD8⁺ T cells into Rag1$^{-/-}$ mice and treated the recipients with TIM3-ProIL2V2 (Fig. 3G). The therapy was more

effective in mice receiving *Havcr3*$^{-/-}$ CD4$^+$ T cells plus WT CD8$^+$ T cells compared to those receiving WT CD4$^+$ T cells plus *Havcr3*$^{-/-}$ CD8$^+$ T cells, further confirming the necessity of TIM3 expression on CD8$^+$ T cells for the antitumor effects of TIM3-ProIL2V2. Collectively, these results pinpoint the dependency of TIM3-ProIL2V2 therapy on the engagement of TIM3 on CD8$^+$ T cells within the tumor, delineating a clear mechanism of action for this promising therapeutic approach.

### Targeting IL-2 induces the proliferation and function of Tim3$^-$CD8$^+$ T cells through Tim3$^+$ TILs

Since the antitumor effect of TIM3-ProIL2V2 depended on pre-existing CD8$^+$ T cells, we further isolated intratumoral CD8$^+$ T cells and investigated the transcriptional signatures at the single-cell level following TIM3-ProIL2V2 monotherapy. We identified five molecularly distinct states of intratumoral CD8$^+$ T cells (Fig. 4A). The proportion of CD8$^+$ T cells within the effector and exhausted stage was significantly increased after TIM3-ProIL2V2 monotherapy, but not CD8$^+$ T cell in stem-like phase (Fig. 4B). However, CD8$^+$ T cell in stem-like and also effector stage expressed high level of proliferation as indicated by strong positive for Ki67, while expressing relatively low levels of *Pdcd1* and *Havcr2*. Conversely, CD8$^+$ T cells in exhausted stage expressing high levels of *Pdcd1* and *Havcr2*, showed no *Ki67* expression, indicating a loss of proliferative ability, but still produced effector molecules, including inflammatory cytokines and granzymes, and possibly contributing to the control of tumors (Fig. 4C, D). Our analysis of cell differentiation pathways revealed that CD8$^+$ T cell from both stem-like and effector stage eventually differentiate into exhausted CD8$^+$ T cells (Supplementary Fig. 3A), explaining the increased proportion of TIM3$^{high}$ CD8$^+$ T cells without proliferation, and the effector feature maintaining even at TIM3$^{high}$ stage.

We observed that TIM3-ProIL2V2 therapy enhanced the expression of genes related to pro-inflammatory cytokines and cytokine receptors, such as *Ifng, Il2rg*, *Il2rb*, *Il12r1,* and *Ifngr*, as well as those encoding costimulatory molecules and inhibitory receptor (Fig. 4E and Supplementary Fig. 3B, C). Gene set enrichment analysis further revealed the upregulation of genes associated with the IL-2/STAT5 signaling pathway, which might enhance the IFN-γ response in CD8$^+$ T cells (Supplementary Fig. 3D, E). These findings demonstrate that CD8$^+$ T cells become more responsive to IL-2 stimulation to produce anti-tumor cytokines such as the IFN-γ[29]. To test if such increase of this cytokine may play a crucial role in the antitumor effects of TIM3-ProIL2V2, we blocked IFN-γ signaling pathway using an IFN-γ neutralizing antibody in MC38 tumor-bearing mice treated with TIM3-ProIL2V2, resulting in abrogated antitumor effect. This indicates that IFN-γ is essential for antitumor efficacy of TIM3-ProIL2V2 (Fig. 4F). Taken together, it is possible that TIM3-ProIL2V2 enhances the proliferation of CD8$^+$ T cells at both stem-like cells and early effectors as well as rejuvenating exhausted T cells into the sources of cytokine-producing cells for collectively potent anti-tumor immunity.

### TIM3-ProIL2V2 activates and expands PD-1$^+$TIM3$^-$CD8$^+$ T cells

In our pursuit to understand the enhanced antitumor response elicited by TIM3-ProIL2V2, particularly in contrast to TIM3-IL2V2-MMPs-Rα, we delved into the dynamics of CD8$^+$ T-cell responses in the MC38 tumor model. Remarkably, we observed a substantial better increase in the population of CD8$^+$ T cells within the TME following treatment with TIM3-ProIL2V2 than TIM3-IL2V2-MMPs-Rα (Fig. 5A and Supplementary Fig. 4A, B). Both TIM3-ProIL2V2 and TIM3-IL2V2-MMPs-Rα induced the expansion of TIM3$^+$CD8$^+$ T cells. However, only TIM3-ProIL2V2, but not TIM3-IL2V2-MMPs-Rα promoted an increase in the population of TIM3$^-$CD8$^+$ T cells (Fig. 5A and Supplementary Fig. 4C, D). This suggests that IL-2 may need to be released to expand and activate TIM3$^-$ TILs, rather than being solely delivered in a cis manner to TIM3$^+$ cells. As previously demonstrated, the antitumor efficacy of TIM3-ProIL2V2 is critically dependent on the role of IFN-γ (Fig. 4E). TIM3-ProIL2V2 was able to enhance IFN-γ secretion in CD8$^+$ T cells to a greater extent than TIM3-IL2V2-MMPs-Rα (Fig. 5B and Supplementary Fig. 4E, F), as TIM3-ProIL2V2 induced more IFN-γ secretion in TIM3$^-$CD8$^+$ T cells compared to TIM3-IL2V2-MMPs-Rα (Fig. 5C, D and Supplementary Fig. 4G). More importantly, a higher percentage of Ki67$^+$ cells was observed in TIM3$^-$CD8$^+$ T cells after treatment with TIM3-ProIL2V2 compared to TIM3-IL2V2-MMPs-Rα (Fig. 5E), indicating that TIM3-ProIL2V2 can act on TIM3$^-$ T cells through IL-2V2 release via MMP cleavage. We theorized that unlike TIM3-IL2V2-MMP-Rα, TIM3-ProIL2V2 need to act beyond TIM3$^+$ T cells, engaging TIM3$^-$ T cells, such as PD-1$^+$TIM3$^-$ effector and stem-like T cells. This interaction could lead to their activation, proliferation, and eventual differentiation into more effectors of PD-1$^+$TIM3$^+$ subsets, thereby replenishing and augmenting the pool of both TIM3$^-$ and TIM3$^+$ cells. Our analyses showed increased percentage of effector PD-1$^+$TIM3$^-$CD8$^+$ (Supplementary Fig. 4C, D) and stem-like T cells under TIM3-ProIL2V2 treatment (Fig. 5F and Supplementary Fig. 4H), suggesting released IL-2 could target TIM3$^-$ TILs.

Antigen-specific cytotoxicity mediated by T lymphocytes plays the critical role in tumor eradication. In the MC38-OVA model, TIM3-ProIL2V2 also demonstrated superior antitumor immunity compared to TIM3-IL2V2-MMPs-Rα (Supplementary Fig. 4J) and significantly enhanced the expansion of tumor-specific CD8$^+$ T cells compared to TIM3-IL2V2-MMPs-Rα (Fig. 5G and Supplementary Fig. 4K). Furthermore, tumor-specific CD8$^+$ T cells treated with TIM3-ProIL2V2 exhibited higher Ki67 expression, indicating that TIM3-ProIL2V2 promoted the proliferation of tumor-specific CD8$^+$ T cells. (Supplementary Fig. 4L, M). Tumor-specific CD8$^+$ T cells in TME repeatedly exposed to tumor antigen, most of the tumor specific CD8$^+$ T cells were PD-1$^+$TIM3$^+$exhausted T cells that failed to proliferate[30]. Therefore, TIM3-IL2V2-MMPs-Rα cannot increased number of late stage of tumor-specific PD-1$^+$TIM3$^+$exhausted T cells (Fig. 5G). TIM3-ProIL2V2 could induce more proliferation of tumor-specific TIM3$^-$ T cells and differentiation to tumor-specific TIM3$^+$CD8$^+$ T cells differentiation in comparison to TIM3-IL2V2-MMPs-Rα (Fig. 5G, H). To further confirm that TIM3-ProIL2V2 can induce the proliferation or activation of Tim3$^-$CD8$^+$ T cells, we performed adoptive cell transfer experiments using T cells from CD45.1$^+$ *Havcr2*$^{wt/wt}$ mice and treated the recipients (CD45.1$^-$ *Havcr2*$^{-/-}$ mice) with TIM3-ProIL2V2. We analyzed the bystander effect of TIM3-ProIL2V2 in *Havcr2* knockout mice transferred CD45.1$^+$*Havcr2*$^{wt/wt}$ T cells. The results showed that TIM3-ProIL2V2 expanded the CD45.1$^-$ *Havcr2*$^{-/-}$ CD8$^+$ T cells, which exhibited a higher percentage of Ki67 expression compared with the control group (Fig. 5I, J and Supplementary Fig. 5A, B), and activated CD45.1$^-$ *Havcr2*$^{-/-}$ CD8$^+$ T cells which exhibited a higher percentage of IFN-γ expression (Fig. 5K and Supplementary Fig. 5C, D), demonstrating the bystander effect of TIM3-ProIL2V2. To further assess whether TIM3-ProIL2V2 could enhance the proliferation and differentiation of TIM3$^-$CD8$^+$ T cells, we sorted TIM3$^-$CD8$^+$ T cells from MC38 tumors and treated them with cleaved TIM3-ProIL2V2. Proliferation was measured by cell count, while differentiation was evaluated by TIM3 upregulation. Remarkably, cleaved TIM3-ProIL2V2 significantly increased the number of TIM3$^-$CD8$^+$ T cells within 48 h of treatment (Supplementary Fig. 6A). Furthermore, TIM3$^-$CD8$^+$ T cells differentiated into TIM3$^+$CD8$^+$ T cells (Supplementary Fig. 6B). The rapid induction of TIM3 expression suggests that IL-2 signaling drives this phenotypic transition. Together, these data demonstrate that TIM3-ProIL2V2 not only expands TIM3$^-$CD8$^+$ T cells but also promotes their differentiation into TIM3$^+$CD8$^+$ T cells.

To investigate whether TIM3-ProIL2V2 could reinvigorate PD1$^+$TIM3$^+$CD8$^+$ T cells, we further analyzed the data and found that CD25, a marker of activation, was expressed at higher level in exhausted T cells compared to the control group (Supplementary Fig. 7A–C). More importantly, TIM3-ProIL2V2 was able to increase IFN-γ production in exhausted T cells (Supplementary Fig. 7D–F). Additionally, we tested this in vitro using induced PD1$^+$TIM3$^+$ Tex cells

https://doi.org/10.1038/s41467-025-60463-4

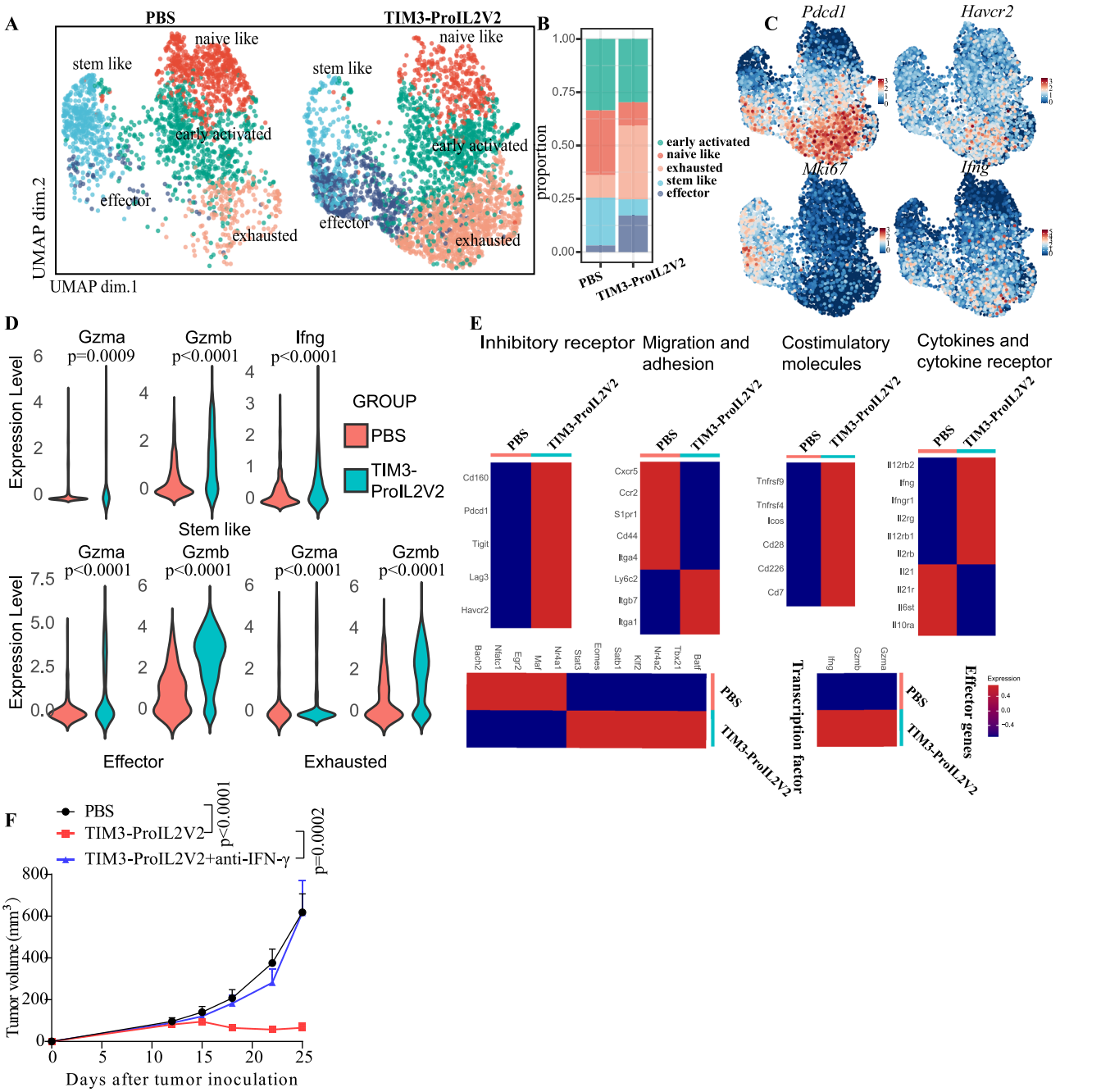


**Fig. 4 | Targeting IL-2 to TIM3$^+$ cells induces the proliferation and function of TIM3$^-$ CD8$^+$ T cells. A–E** MC38 tumor-bearing female C57BL/6 mice ($n = 3$/group) were treated with TIM3-ProIL2V2 (10 μg) on day 16 after tumor inoculation. Three days later, CD8$^+$ cells were sorted for single-cell RNA sequencing. **A** UMAP visualization of intratumoral CD8$^+$ T cells colored according to specific treatment effect. **B** The proportion change of different stages within CD8$^+$ T cells after TIM3-ProIL2V2 monotherapy. **C** Normalized expression of *Pdcd1*, *Havcr2*, *Mki67*, and *Ifng* is shown within the five clusters. **D** The mean relative expression of specific genes in effector, exhausted, and stem like CD8$^+$ T cells between PBS and TIM3-ProIL2V2 groups. **E** Expression of inhibitory receptor, migration and adhesion, costimulatory molecules, cytokines and cytokine receptor, effector genes, transcription factor across cells in TIM3-ProIL2V2 and PBS. **F** Female C57BL/6 mice ($n = 6$/group) were inoculated with 5 × 105 MC38 cells i.p. treated with 10 μg TIM3-ProIL2V2 on day 14 and 17 post-tumor inoculation. For IFN-γ neutralization, 500 μg anti- IFN-γ was administrated on the same day of treatment initiation and then twice a week for 2 weeks. *P* value was determined by two-sided Wilcoxon rank sum test with continuity correction (**D**). Data is shown as mean ± SEM and representative of at least two independent experiments. *P* value was determined by unpaired two-tailed *t* tests (**F**).

isolated from mouse spleens. The PD1$^+$TIM3$^+$ Tex cells were reactivated and produced more IFN-γ after treatment with TIM3-ProIL2V2 (Supplementary Fig. 7G, H). These results demonstrate that TIM3-ProIL2V2 can reinvigorate PD1$^+$TIM3$^+$ Tex cells. These findings collectively highlight TIM3-ProIL2V2's ability to bind to TIM3-positive T cells, reactivating exhausted PD-1$^+$TIM3$^+$ T cells while simultaneously activating and expanding the PD-1$^+$TIM3$^-$CD8$^+$ T cell and stem-like T cell populations. This creates a continuous source of TIM3$^+$IFN-γ$^+$ and tumor-specific T cells, substantially amplifies the antitumor effector cells.

## TIM3-ProIL2V2 could overcome immune checkpoint blockade resistance in cold tumors

Immune checkpoint blockade (ICB) resistance after PD-1/L1 therapy has become one major clinical problem, especially in cold tumor[31,32]. The B16F10 melanoma model is widely recognized as a classical cold

https://doi.org/10.1038/s41467-025-60463-4

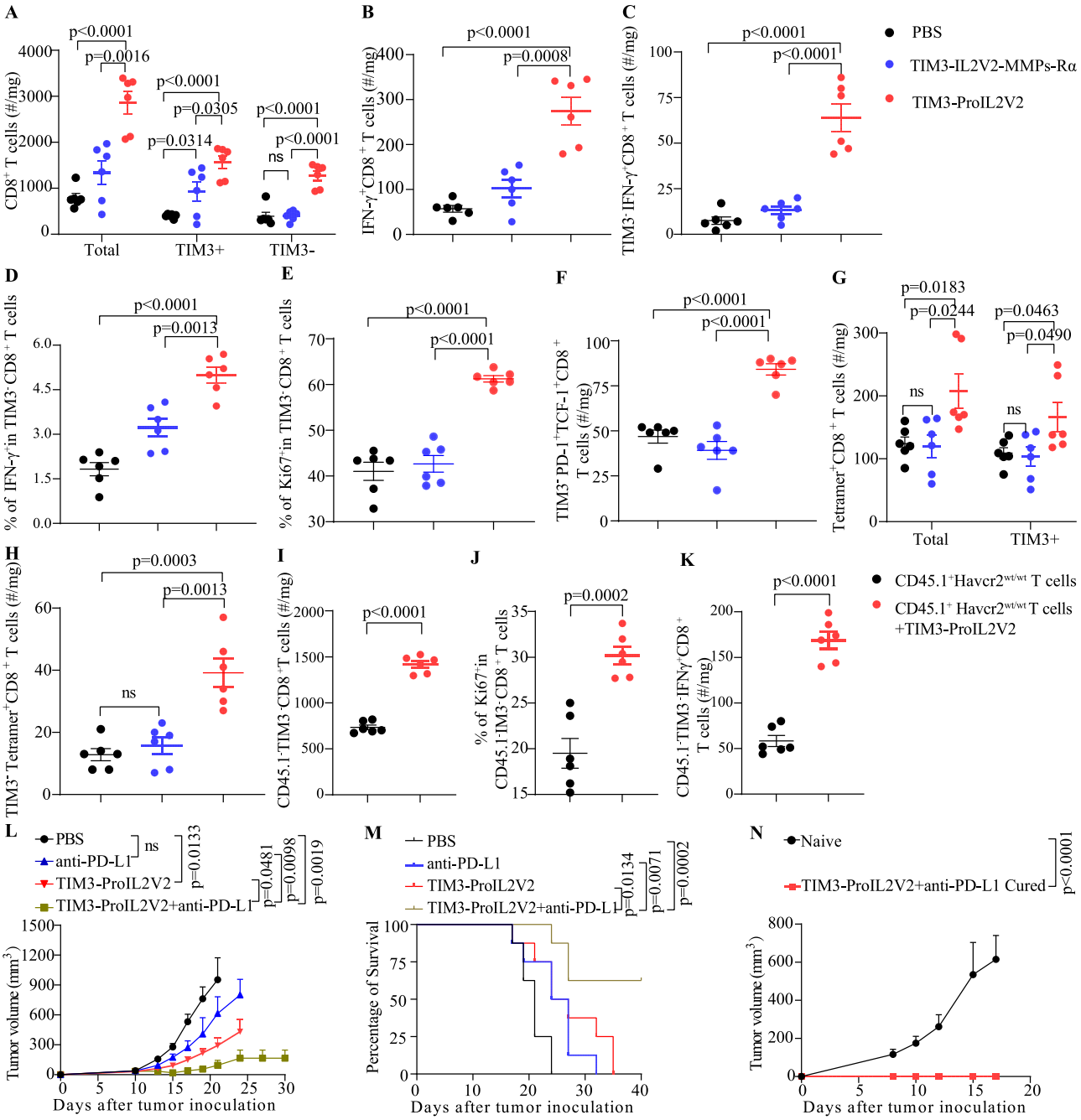


**Fig. 5 | TIM3-ProIL2V2 activates and expands TIM3$^-$ CD8$^+$T cells to overcome PD-1 resistance. A–F** MC38 tumor-bearing female C57BL/6 mice ($n = 6$/group) were treated with 10 μg TIM3-ProIL2V2 or TIM3-IL2V2-MMPs-Rα on day 16. After 3 days, mice were intraperitoneally injected with 50 μl of brefeldin A solution (BFA, 5 mg/ml). Six hours later, the mice were sacrificed and tumor tissues were collected, and FACS analysis was performed. The number of intratumoral total CD8$^+$T cells/TIM3$^+$ CD8$^+$T cells and TIM3$^-$CD8$^+$T cells (**A**), IFN-γ$^+$CD8$^+$T cells (**B**), IFN-γ$^+$TIM3$^-$CD8$^+$ T cells (**C**), and PD-1$^+$TIM3$^-$TCF1$^+$CD8$^+$ T cells (**F**) were measured by flow cytometric analysis. The percentage of IFN-γ$^+$ (**D**) and Ki67$^+$ (**E**) in TIM3$^-$CD8$^+$T cells were measured by flow cytometric analysis. **G**, **H** MC38-OVA tumor-bearing female C57BL/6 mice ($n = 6$/group) were treated with 10 μg TIM3-ProIL2V2 on day 16 after tumor inoculation. The mice were sacrificed and tumor tissues were collected 72 h after the first injection. The number of OVA-specific CD8$^+$ T cells were measured by flow cytometric analysis. **I–K** MC38 tumor-bearing female *CD45.2*$^+$ *Havcr2*$^{-/-}$ mice ($n = 6$/group) were transferred with $2 \times 10^6$ *CD45.1*$^+$ *Havcr2*$^{wt/wt}$ T cells on day 2 after tumor inoculation, followed by treatment with TIM3-ProIL2V2 or PBS on day 12 after tumor inoculation. The mice were sacrificed and tumor tissues were collected 72 h after TIM3-ProIL2V2 treatment. The number of intratumoral CD45.1$^-$TIM3$^-$CD8$^+$ T cells (**I**) and IFN-γ$^+$CD45.1$^-$TIM3$^-$CD8$^+$ T cells (**K**) were measured by flow cytometric analysis. The percentage of Ki67$^+$ (**J**) in CD45.1$^-$TIM3$^-$CD8$^+$ T cells were measured by flow cytometric analysis. **L**, **M** B16F10 bearing female C57BL/6 mice ($n = 8$/group) were i.p. treated with 25 μg TIM3-ProIL2V2 and/or 150 μg anti-PD-L1 twice on day 10 and 13 after tumor inoculation. Tumor volume (**G**) was measured as indicated and the mouse survival curve was shown in (**H**). **N** B16F10 bearing female C57BL/6 mice were treated with TIM3-ProIL2V2 and anti-PD-L1. 30 days after treatment, cured mice ($n = 5$/group) were re-challenged with $2 \times 10^6$ B16F10 cells. Data are shown as mean ± SEM and representative of two to three independent experiments. *P* value was determined by unpaired two-tailed *t* tests (**A–L**, **N**). Statistical analysis of survival curve was compared using a log-rank test (**M**).

tumor model, characterized by limited T cell infiltration and low responsiveness to immune therapies, including ICB treatment[33,34]. Our single-cell and FACS analyses revealed increases in both PD-1$^+$TIM3$^-$ and PD-1$^+$TIM3$^+$ T cell subsets post-TIM3-ProIL2V2 treatment, suggesting a potential counteracting effect of PD-1 signaling on the therapy. We speculated that TIM3-ProIL2V2 could overcome PD-1/L1 resistance. To address if TIM3-ProIL2V2 can overcome ICB resistance[35], we combined TIM3-ProIL2V2 with anti-PD-L1 antibodies in a B16F10 tumor model, which remarkably curtailed tumor growth and, in many cases, led to complete tumor eradication (Fig. 5L, M). Thus TIM3-ProIL2V2 indeed overcome PD-1/L1 resistance by not only more effectively managed tumor growth but also established a better potent memory immune response than PD-L1 alone, preventing tumor recurrence upon rechallenge (Fig. 5N). Since B16F10 is a rather cold tumor model, TIM3-ProIL2V2 might become a potent strategy to overcome ICB resistance in cold tumors, unmet medical needs.

### TIM3-ProIL2V2 could assist T cell therapy and radiation therapy

The efficacy of T cell therapy in solid tumors is often hampered by their ability to navigate, penetrate, activate, or expand inside the immunosuppressive TME[31,36]. We hypothesized that the scarcity of IL-2 was the key defect that limited their activation and expansion. In this context, we explored the potential of TIM3-ProIL2V2 to enhance the effectiveness of T cell therapy. T cell therapy is not very effective for a B16-OVA tumor model in CD45.1$^-$ mice, we test if TIM3-ProIL2V2 treatment can provide sufficient cytokines for CD45.1$^+$OT-I$^+$CD8$^+$ T cells in advanced B16-OVA tumor model. Additional IL-2 inside TME overcame the resistance to T cell therapy as the combination treatment significantly suppressed tumor growth and prolonged survival (Fig. 6A, B) without inducing weight loss or observed side effects (Supplementary Fig. 8A). Impressively, some mice have even achieved complete tumor clearance and protected against tumor recurrence (Fig. 6C). The results suggested that the systemic delivery of TIM3-Rα-MMPs-IL2V2 could potently activate and expand few TILs and develop memory immune response against cold tumor.

In order to understand the enhanced antitumor response of T cell therapy elicited by TIM3-ProIL2V2, we further investigated how the CD8$^+$ T cell responses, especially CD45.1$^+$OT-I$^+$CD8$^+$ T cells were reshaped to promote the antitumor efficacy in the B16-OVA tumor model. We found that the frequency of Tetramer$^+$CD8$^+$ T cells, including both CD45.1 positive and negative populations, increased significantly (Fig. 6D and Supplementary Fig. 8B). Flow cytometric analysis of tumor tissues revealed an increase in the transferred CD45.1$^+$OT-I$^+$CD8$^+$ T cells following TIM3-ProIL2V2 treatment (Fig. 6E and Supplementary Fig. 8C). Significantly higher levels of Ki67 expression were observed in CD45.1$^+$OT-I$^+$CD8$^+$ T cells within the tumor following TIM3-ProIL2V2 treatment (Fig. 6F), indicating that TIM3-ProIL2V2 effectively promoted the proliferation of CD45.1$^+$OT-I$^+$CD8$^+$ T cells. A significant increase in the number of CD45.1$^+$TIM3$^-$PD-1$^+$CD8$^+$ T cells, along with higher Ki67 expression, was observed following TIM3-ProIL2V2 treatment. This finding suggests that TIM3-ProIL2V2 promotes the proliferation of the CD45.1$^+$TIM3$^-$PD-1$^+$CD8$^+$ T cell subset (Fig. 6G and I and Supplementary Fig. 8D). However, the proportion of CD45.1$^+$TIM3$^-$PD-1$^+$CD8$^+$ T cells within the CD45.1$^+$OT-I$^+$CD8$^+$ T cell population decreased (Fig. 6H). We proposed that the most of CD45.1$^+$TIM3$^-$PD-1$^+$CD8$^+$ T cells were differentiated into CD45.1$^+$TIM3$^+$PD-1$^+$CD8$^+$ T cells in the tumor following TIM3-ProIL2V2 treatment, leading to a decreased proportion of TIM3$^-$PD-1$^+$CD8$^+$ T cells due to the lack of new exogenous cell supplementation. We further analyzed the endogenous CD45.1$^-$Tetramer$^+$CD8$^+$ T cells and found both the number and proportion of CD45.1$^-$Tetramer$^+$TIM3$^-$PD-1$^+$CD8$^+$T cells within the CD45.1$^-$ Tetramer$^+$CD8$^+$ T cells were increased in tumor (Fig. 6J and Supplementary Fig. 8E). We also observed that TIM3-ProIL2V2 treatment resulted in a higher frequency of Tetramer$^+$ CD8$^+$ T cells in the spleen and lymph nodes of B16-OVA-bearing mice, further supporting the generation of anti-tumor memory immune responses (Fig. 6K, L and Supplementary Fig. 8F, G).

Local radiation is clinically used to rapidly reduce tumor burden but the relapse is the major problem[37,38]. We also investigated if TIM3-ProIL2V2 can overcome radiotherapy relapse for advanced cancer. Our studies demonstrated that combining TIM3-ProIL2V2 with radiotherapy markedly enhanced the antitumor response beyond what was achieved with either treatment alone, effectively curbing tumor growth (Fig. 6M). Radiation therapy can effectively eliminate tumor cells and control tumor growth. However, immune cells are also sensitive to radiation, and we found that the number of CD8$^+$ T cells significantly decreased following radiation treatment, contributing to tumor immune desertification. This impairs further tumor control, leading to relapse in patients who have undergone radiation therapy. Therefore, restoring T cell function and expanding their population is crucial for enhancing the effectiveness of radiation treatment in clinical settings. Based on these findings and the results we previously presented, we believe TIM3-ProIL2V2 could effectively address the needs of radiation therapy. In this context, we investigated the potential of TIM3-ProIL2V2 to enhance T cell numbers and function, positioning it as a potent agent to improve the efficacy of radiation therapy and T cell therapy in advanced cancers. Additional TIM3-ProIL2V2 restored the reduced CD8$^+$ T cell number after radiation and induced more IFN-γ expression (Fig. 6N, O). These findings illuminate the potential of TIM3-ProIL2V2 to amplify the antitumor efficacy of T cell therapy in cold tumors and suggest a promising combination strategy with radiotherapy to overcome the limitations of traditional cancer treatments.

### TIM3-ProIL2V2 could control tumor in humanized tumor models

To test the translational potential of TIM3-ProIL2V2 therapy in more clinically relevant model, we employed humanized tumor models to evaluate anti-human TIM3-ProIL2V2 against human tumors. Firstly, we selected *human havcr2* gene knock-in mice to test anti-human TIM3-ProIL2V2 and observed remarkable success in eradicating tumors in a majority of human *havcr2* gene knock-in mice implanted with established MC38 tumors (Fig. 7A, B). This promising outcome was characterized not only by the complete clearance of tumors but also by the establishment of a robust memory immune response, effectively preventing any recurrence of the tumor (Fig. 7C). Human *havcr2* gene knock-in mice have some limitations since only *havcr2* gene is human to replace mouse while other cells and genes are same with normal mouse. We performed adoptive cell transfer experiments using T cells from WT and human *havcr2* knock-in mice, treating the recipients with species-specific (anti-human or mouse) TIM3-ProIL2V2. The therapy was effective in mice receiving T cells compatible with the therapeutic antibody's target, thereby confirming the necessity of TIM3 expression on T cells for the antitumor effects of TIM3-ProIL2V2 (Fig. 7D). To test if human T cells might also respond to TIM3-ProIL2V2 well, we transferred a human peripheral blood mononuclear cell (PBMC) into NSG mice, which all T cells were from human. Treatment with human TIM3-ProIL2V2 in this model also led to significant tumor growth inhibition (Fig. 7E), reinforcing the therapeutic potential observed in the human *havcr2* knock-in model. Additionally, we analyzed the phenotypes of TILs under different conditions. We found that treatment with human TIM3-ProIL2V2 resulted in a significant increase in both TIM3$^+$ CD8$^+$ T cells and TIM3$^-$, including TIM3$^-$PD-1$^+$TCF-1$^+$CD8$^+$ T cells (Fig. 7F, G). These findings collectively underscore the potent antitumor capabilities of human TIM3-ProIL2V2 within a human T cell context, suggesting its promising prospects for clinical application in cancer immunotherapy.

## Discussion

To augment the antitumor efficacy and mitigate the toxicity of IL-2, various engineered Pro-IL2 incorporating an obstructive IL-2 receptor

https://doi.org/10.1038/s41467-025-60463-4

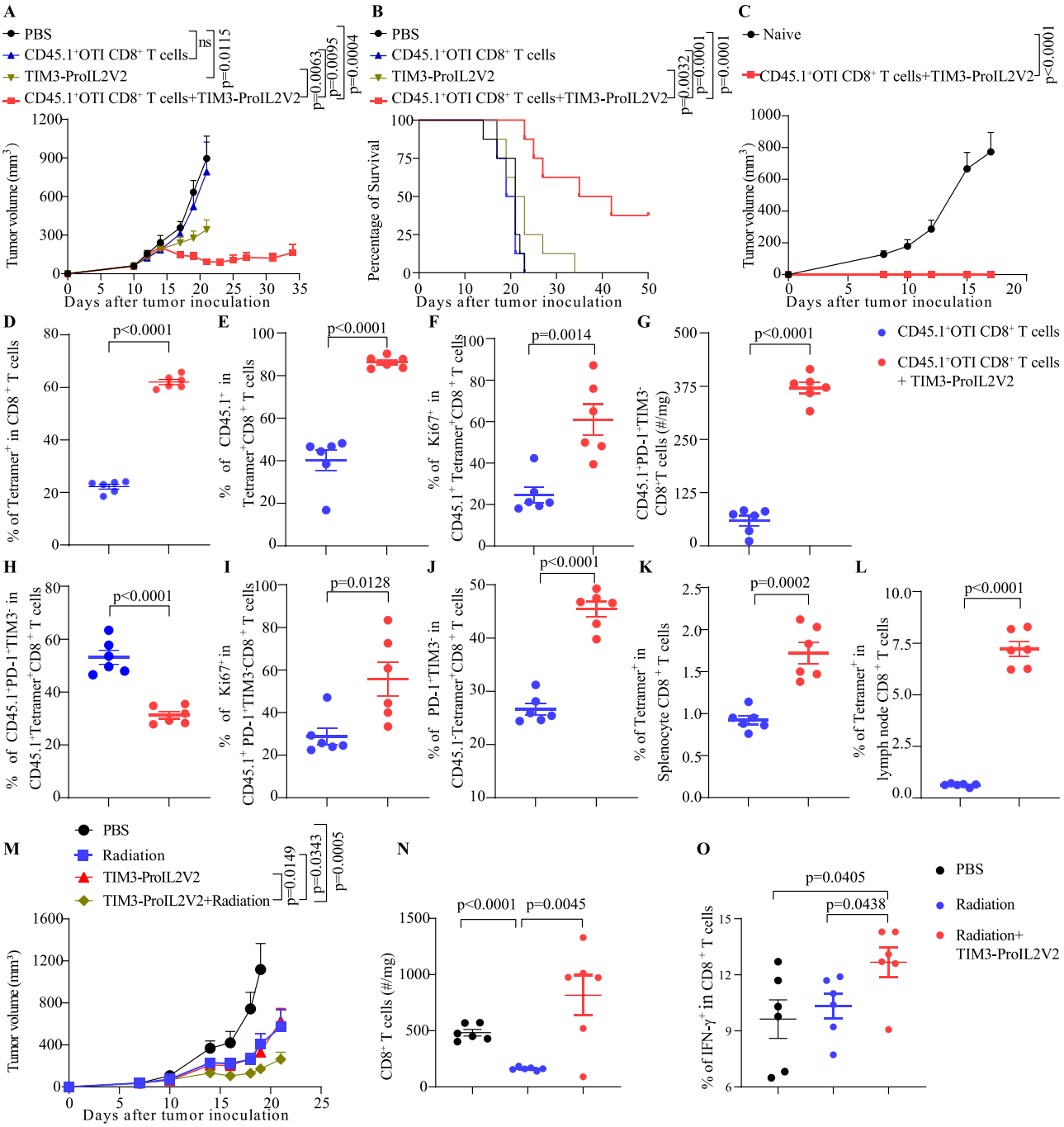


**Fig. 6 | TIM3-Pro-IL2V2 could control cold tumor. A, B** $2 \times 10^6$ stimulated CD45.1$^+$OT-I$^+$CD8$^+$ T cells were adoptively transferred to B16F10-OVA bearing female C57BL/6 mice ($n = 8$/group) 10 days after tumor inoculation. 25 μg TIM3-ProIL2V2 was administrated on day 12 and 15 after tumor inoculation. Tumor volume (**A**) was measured as indicated and the mouse survival curve was shown in (**B**). **C** 30 days after treatment with OT-I$^+$CD8$^+$ T cells and TIM3-ProIL2V2, cured mice ($n = 3$/group) were re-challenged with $2 \times 10^6$ B16F10-OVA cells. **D**–**L** B16F10-OVA bearing female C57BL/6 mice ($n = 6$/group) were treated with OT-I$^+$CD8$^+$ T cells with or without 25 μg TIM3-ProIL2V2 on day 12 and 15 after tumor inoculation. The mice were sacrificed and tumor tissues were collected 24 h after second injection. The percentage of total OVA-specific CD8$^+$T cells (**D**), percentage of CD45.1$^+$OT-I CD8$^+$ T cells in total OVA-specific CD8$^+$T cells (**E**), percentage of Ki67$^+$ in CD45.1$^+$OT-I CD8$^+$ T cells (**F**), number and percentage of CD45.1$^+$OT-I PD-1$^+$TIM3$^-$CD8$^+$ T cells in CD45.1$^+$OT-I CD8$^+$ T cells (**G** and **H**), percentage of Ki67$^+$ in CD45.1$^+$OT-I PD-1$^+$TIM3$^-$CD8$^+$ T cells (**I**), percentage of CD45.1$^-$Tetramer$^+$ PD-1$^+$TIM3$^-$CD8$^+$ T cells in CD45.1$^-$ Tetramer$^+$ CD8$^+$ T cells (**J**), percentage of total OVA-specific CD8$^+$T cells in splenocyte CD8$^+$ T cells (**K**) and in lymph node CD8$^+$ T cells (**L**). **M** B16F10 bearing female C57BL/6 mice were treated with PBS ($n = 6$), 12 Gy Radiation ($n = 8$), 25 μg TIM3-ProIL2V2 ($n = 6$) or 12 Gy Radiation + 25 μg TIM3-ProIL2V2 ($n = 8$) on day 9 and 12 after inoculation. Tumor volume was measured as indicated. **N**–**O** B16F10 bearing female C57BL/6 mice ($n = 8$/group) were treated 12 Gy Radiation on day 9 and/or 25 μg TIM3-ProIL2V2 on day 9 and 12 after tumor inoculation. The mice were sacrificed and tumor tissues were collected 24 h after second injection. The number of CD8$^+$ T cells (**N**) and percentage of IFN-γ$^+$CD8$^+$ T cells (**O**) were measured by FACS. Data are shown as mean ± SEM and representative of two to three independent experiments. *P* value was determined by unpaired two-tailed *t* tests (**A**, **C**–**O**). Statistical analysis of survival curve was compared using a log-rank test (**B**).

https://doi.org/10.1038/s41467-025-60463-4

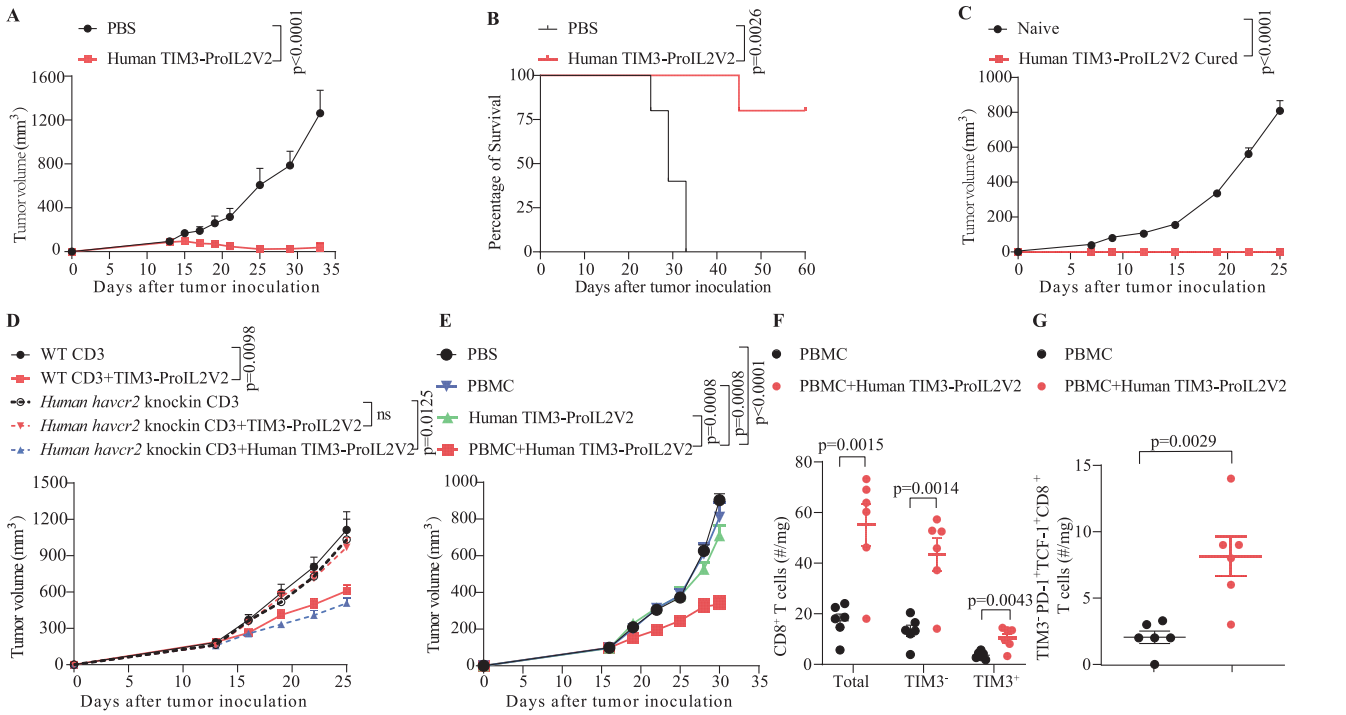


**Fig. 7 | TIM3-ProIL2V2 could control tumor in humanized tumor model.** **A**, **B** Female Human *Havcr2* knockin mice ($n = 5$/group) were inoculated with $5 \times 10^5$ MC38 tumor cells and i.p. treated with 20 μg human TIM3-ProIL2V2 on day 14 and 17 after tumor inoculation. Tumor volume (**A**), and survival (**B**) were recorded as indicated. **C** MC38 bearing female Human *Havcr2* knockin mice were treated with 20 μg human TIM3-ProIL2V2 on day 14 and 17 after tumor inoculation. 30 days after treatment, cured mice ($n = 4$/group) were re-challenged with $2 \times 10^6$ MC38 cells. **D** $3 \times 10^6$ $CD3^+$ T cells from the spleens of C57BL/6 mice or Human *Havcr2 knockin* mice ($n = 6$/group) were adoptively transferred to MC38 bearing female *Rag1*$^{-/-}$ mice 5 days after tumor inoculation. 10 μg TIM3-ProIL2V2 or human TIM3-ProIL2V2 was administrated on day 12 and 15 after tumor inoculation. **E** Female NSG mice ($n = 5$/group) were subcutaneously inoculated with $2 \times 10^6$ A431 tumor cells. Mice were i.v. injected with $10^7$ human PBMC for human immunity construction on day 7 after tumor inoculation. Tumor-bearing mice were treated with 20 μg human TIM3-ProIL2V2 on days 12, 15, and 18 after tumor inoculation. Tumor volume (**E**) was measured as indicated. **F**, **G** Mice ($n = 6$/group) were i.v. injected with $10^7$ human PBMC for human immunity construction on day 7 after tumor inoculation. Tumor-bearing mice were treated with 20 μg human TIM3-ProIL2V2 on days 12 after tumor inoculation. The mice were sacrificed and tumor tissues were collected 72 h after TIM3-ProIL2V2 treatment. The number of intratumoral total $CD8^+$ T cells, $TIM3^-CD8^+$T cells, $TIM3^+CD8^+$ T cells (**F**) and stem-like $CD8^+$ T cells ($TIM3^-PD\text{-}1^+TCF1^+CD8^+$ T cells) (**G**) were measured by flow cytometric analysis. Data are shown as mean ± SEM and representative of two to three independent experiments. *P* value was determined by unpaired two-tailed *t* tests (**A**, **C**–**G**). Statistical analysis of survival curve was compared using a log-rank test (**B**).

were developed[22,39]. These precursors are activatable by tumor-associated MMPs[17]. Despite the extended half-life and reduced adverse effects of Pro-IL2[40], its limited efficacy and suboptimal targeting of the TME present significant hurdles. Enhancing the specificity of Pro-IL2 delivery to tumor-specific T cells while minimizing systemic toxicity remains a pivotal challenge in IL-2-based cancer immunotherapy. Concurrently, monoclonal antibodies against TIM3 are under investigation in phase III clinical trials with limited anti-tumor activity[41,42]. Moreover, the high expression of TIM3 on TILs could provide IL-2 targeting strategies by anti-TIM3 antibody. To test that, we fused pro-IL-2 to the Fc region of anti-TIM3 antibodies (TIM3-Rα-MMP-IL2V2 vs TIM3-IL2V2-MMP-Rα). IL2V2, a low pH-selective IL-2 mutein with enhanced affinity for IL-2Rβ on effector cells, was designed to function optimally within the acidic TME. We hypothesized that IL-2V2, when conjugated to anti-TIM3, would facilitate cis targeted delivery specifically to $TIM3^+$ TILs inside harsh low pH TME. Unexpectedly, the released IL-2 from TIM3-Rα-MMP-IL2V2 led to better anti-tumor activities than cis delivered IL-2 of TIM3-IL2V2-MMP-Rα. TIM3-Rα-MMP-IL2V2 promoted the activation of not only $TIM3^+$ exhausted T cells but also proliferation, and differentiation of rest $TIM3^-$ T cells, including $PD1^+TIM3^-$ effector $CD8^+$ T cells and stem-like $CD8^+$ T cells, which in turn supported a sustained source of $TIM3^+$ effector, promoting the uptake of more TIM3-ProIL2V2 by the tumor. Due to the increase of $TIM3^{high}CD8^+$ T cells in tumors, we found that TIM3 on T cells, rather than on DC or macrophages, was crucial for TIM3-ProIL-2 targeting. Released IL2V2 thus, enhanced the responses across a broader spectrum of TIL subsets from progenitor, early, and late stages of effector cells, boosting stronger antitumor immune responses (Fig. 8). Collectively, these findings demonstrate that tumor-activating low pH resistant IL2 rejuvenates intratumoral both $TIM3^+$ and $TIM3^-CD8^+$T cells responses through $TIM3^+CD8^+$T cells.

Cis effect of low-affinity IL-2 by high affinity of PD-1 antibody has been shown to be more potent anti-tumor immunity than non-cis form by many groups[10,22]. Different with low-affinity IL-2 mutein used in PD-1-cis low-affinity IL-2, released IL2 from TIM3 antibody binds to IL-2R on $CD8^+$T cells from both $TIM3^+$ and $TIM3^-$ TILs without detectable Treg-associated IL-2 trapping (Supplementary Fig. 4I)[43,44]. PD-1 could express on many early activated T cells outside TME while TIM3 is expressed more strictly to late stage of effector inside TME. Consistently, cancer patients frequently encounter various infections[45,46], vaccinations[47], and multiple cancer treatments, such as radiation therapy and ICB therapy[48,49]. These factors contribute to the upregulation of more PD-1 than TIM3 on circulating T cells[50,51]. Consequently, a PD-1-cis low-affinity IL-2 formulation could non-selectively bind to more circulating PD-1-positive T cells, potentially inducing severe peripheral toxicity. Thus, anti-TIM3 antibody might provide lower toxicity, involves direct delivery of IL-2 inside TME.

PD-1 inhibitors, serving as the primary treatment for various cancers, are commonly administered in high doses[52]. These inhibitors bind to the PD-1 antigen on T cells, effectively blocking the binding sites for PD-1-cis low-affinity IL-2. Consequently, patients receiving PD-1 antibodies are unlikely to benefit from PD-1-cis low-affinity IL-2

https://doi.org/10.1038/s41467-025-60463-4

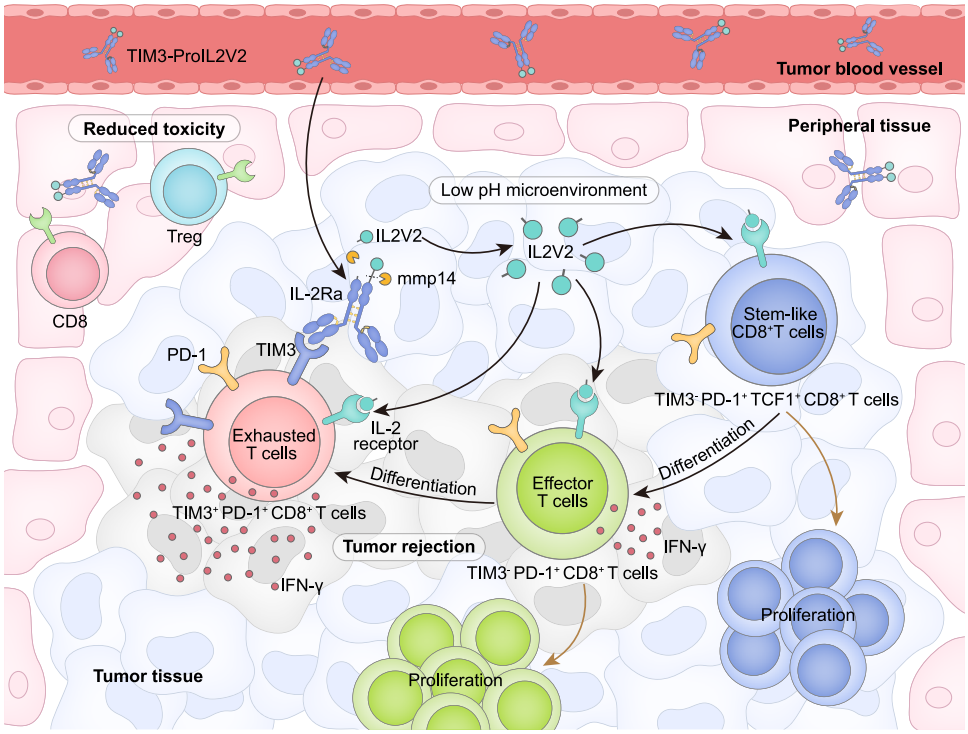


**Fig. 8 | Schematic of hypothesized working model.** Due to tumor targeting, TIM3-ProIL2V2 bound to TIM3$^+$ TILs and enhanced the specificity of ProIL2V2 delivery to tumor-specific T cells while minimizing systemic toxicity. After MMPs digestion inside TME, the released IL-2 from TIM3-ProIL2V2 promoted the activation of not only TIM3$^+$ exhausted T cells but also proliferation and differentiation of rest TIM3$^-$ T cells, including PD1$^+$TIM3$^-$ effector CD8$^+$ T cells and stem-like CD8$^+$ T cells. Released IL2V2 thus, enhances the responses across a broader spectrum of TIL subsets from progenitor, early, and late stages of effector cells, boosted stronger antitumor immune responses.

therapy. In contrast, we observed that additional TIM3-ProIL2V2 overcome PD-1 therapy resistance.

Adaptive transferring large number of T cell-based therapy might also face limited IL-2 in TME leading to rapid exhaustion. Our findings have further illustrated that the TIM3-ProIL2V2 complex can effectively synergize with the adoptive transfer of tumor-reactive T cells, leading to controlled tumor growth even for cold tumors. By utilizing tumor targeting and the controlled release of IL2V2 within the TME, the TIM3-ProIL2V2 complex demonstrated a significant synergistic effect when combined with the transfer of smaller number of tumor reactive T cells, highlighting its potential to rejuvenate TILs without their toxicity.

Deviating from the traditional cis configuration of fusion proteins, TIM3-ProIL2V2 capitalizes on the targeted engagement of intratumoral T cells via the anti-TIM3 moiety, coupled with the enhanced affinity of IL2V2 for IL-2Rβ. This dual functionality facilitates the activation of a broad spectrum of intratumoral cytotoxic T lymphocytes, promoting tumor rejection while minimizing systemic toxicity. Furthermore, we have validated that the humanized TIM3-ProIL2V2 formulation exhibits potent antitumor activity across diverse humanized tumor models, underscoring its potential viability for clinical translation and therapeutic application.

## Methods

C57BL/6 and C57BL/6 *Rag1* KO mice were purchased from GemPharmatech Co., Ltd (Stock Number: N000013 and T004753, respectively). Human *havcr2* knockin mice were obtained from the Shanghai Model Organisms Center, Inc. (Stock Number: NM-HU-00054). *Zbtb46*-Cre mice were from the Jack Laboratory (Stock Number: 028538). *Cd4*-Cre mice were from Taconic (Stock Number: 4196)[53]. *Lyz2*-Cre and *havcr2* $^{fl/fl}$ mice were from Cyagen Bioscience Inc. (Stock Number: C001358 and S-CKO-03616, respectively). All experiments used mice aged 7–8 weeks. All mice were maintained under specific pathogen-free facility in Tsinghua university. Animal care and experiments were carried out under institutional protocol and guidelines. All studies were approved by the Animal Care and Use Committee of Tsinghua university.

### Cell lines and reagents

MC38, B16F10, and CTLL-2 were purchased from the American Type Culture Collection. B16F10-OVA was selected from signal-cell clones after transfection by lentivirus expressing OVA. MC38, B16-F10, and B16F10-OVA were cultured in Dulbecco's modified Eagle's medium, supplemented with 10% heat-inactivated fetal bovine serum, penicillin (100 U/ml), and streptomycin (100 μg/ml) under 5% $CO_2$ at 37 °C. CTLL-2 was maintained in RPMI 1640 with established protocols. Invitrogen FreeStyle 293-F cells (R79007) were cultured in SMM 293-TII medium (M293TII, Sino Biological). Anti-CD4 antibody (GK1.5), anti-CD8 antibody (53–5.8), anti-NK1.1 antibody (PK136), anti-CSF1R (AFS98), anti-IFNγ antibody (XMG1.2), anti-PD-L1 antibody (10 F.9G2), and anti-IL-2Rβ (TM-β1) were purchased from Bio X Cell. FTY720 was purchased from Sigma-Aldrich.

### Tumor inoculation and treatment

MC38 cells ($5 \times 10^5$), B16F10 cells ($3 \times 10^5$), B16F10-OVA cells ($3 \times 10^5$), and A431 ($2 \times 10^6$) were subcutaneously injected into the right flank of mice. The tumor volume was measured twice a week and calculated by length × width × height/2. After the tumors were established, mice received intraperitoneal injections of PBS, anti-TIM3 antibody, ProIL2V2, TIM3-IL2V2, TIM3-IL2V2-MMPs-Rα, TIM3-IL2V2-Rα, TIM3-Rα-MMPs-IL2V2, and TIM3-Rα-MMPs-IL2V2 and TIM3-Rα-MMPs-IL2, respectively, every 3 days for a total of two injections unless otherwise indicated. To inhibit lymphocyte trafficking, FTY720 was administrated at 20 μg one day before treatment initiation and then every

other day for 2 weeks. For specific depletion of CSF1R, NK1.1, $CD4^+$, and $CD8^+$ T cell, 500 μg anti-CSF1R, 200 μg anti-NK1.1, 200 μg anti-CD4 or 200 μg anti-CD8 was administrated one day before treatment initiation and then twice a week for 2 weeks. For IFN-γ neutralization, 500 μg anti- IFN-γ was administrated on the day of treatment initiation and then twice a week for 2 weeks. The humane endpoints are defined as no greater than 1500 $mm^3$ for the B16F10, B16F10-OVA, and A431 tumor model and no greater than 800 $mm^3$ for the MC38 and MC38-OVA tumor model. The euthanasia procedure for mice involves $CO_2$ anesthesia followed by cervical dislocation.

### MMP cleavage and bioactivity of ProIL2V2

Recombinant human MMP14 (R&D Systems) was activated with rhFurin in an activation buffer at 37 °C for 1 h, then incubated with 1 ng/μL AEBSF (R&D Sciences) for 15 min following the manufacturer's instructions. ProIL2V2 was cocultured with activated rhMMP14 in cleavage assay buffer overnight at 37 °C. Cleavage Assay Buffer consisted of 50 mM tris, 3 mM CaCl2, and 1 μM ZnCl2 (pH 7.5). The bioactivity of the digested ProIL2V2 was assessed by measuring the proliferation of the CTLL-2 reporter cell line.

### Fluorescence imaging

TIM3-ProIL2V2 was labeled with Sulfo-Cy5 NHS ester (RuixiBiotechCo.Ltd) and purified by removing the unbound Cy5. Cy5 labeled TIM3-ProIL2V2 or Claudin-ProIL2V2 was intravenously injected into C57BL/6 mice bearing MC38 tumors. The accumulation of Cy5-labeled protein within tumors was measured with IVIS Spectrum (PerkinElmer). The fluorescence imaging data was analyzed with Living Image software (PerkinElmer).

### KM plotter database analysis

KM plotter website is an online survival analysis tool that can be used to assess the effect of single genes on cancer prognosis. Kaplan–Meier curve was generated by comparing patients with high vs low HAVCR2 or IL-2 expression levels within advanced colorectal adenocarcinoma, or breast cancer in KM plotter website. (KM plotter; https://www.kmplot.com/analysis/)

### Flow cytometry

Mice were intraperitoneally injected with 50 μl of brefeldin A solution (BFA, 5 mg/ml) six hours before sacrificing mice[26,54]. Tumor tissues were collected, cut into small pieces, and digested with 100 μg/ml DNase I (Roche) and 1 mg/ml collagenase IV (Roche) at 37 °C for 40 min. The digested tumors were then passed through a 70 μm cell strainer to make single-cell suspensions. Single cells were blocked with anti-CD16/32 Ab (clone 93) for 30 min and then stained with specific antibodies for 30 min on ice. For intracellular staining, samples were fixed, permeabilized, and stained with specific antibodies for 1 h on ice. All fluorescent-labeling mAbs were purchased from BioLegend or eBioscience. Samples were analyzed on a FACS Calibur or Fortessa flow cytometer (BD Biosciences). Data were analyzed using FlowJo software (TreeStar).

### Sample preparation for scRNA-seq

We used the Chromium Next GEM Single Cell 3' Kit (10× Genomics) to generate scRNA-seq libraries according to the manufacturer's protocol. FACS sorting of cells from three biological replicates labeled with CD45 Antibody (BioLegend). The sorted cells were loaded onto a Chromium single-cell chip to generate barcoded nucleic acid fragments. The amplified cDNA was used to generate gene expression libraries. These libraries were sequenced on an Illumina NovaSeq 6000.

### Data analysis for scRNA-seq

Fastq files of gene expression were aligned to the reference genome using Cellranger counting (Cell Ranger v.7.1.0)[55], performing simultaneous filtering, barcode counting, and UMI counting. R (v4.2.2) and Seurat (v4.1.0[56] were used for downstream analysis of the data. Briefly, cells with a mitochondrial gene percentage below 2% were included. Data for genes detected between 200 and 4000 cells were retained and used for downstream analysis. Use the NormalizeData and ScaleData functions to normalize and scale the data, respectively. Variable genes were identified using FindVariableFeatures. Determine UMAP and neighbors from the first 30 PCAs using the RunUMAP function and the FindNeighbors function, respectively. Clusters were identified using the shared nearest neighbor algorithm in Seurat and t-SNE plots were generated based on selected PCA dimensions. Use the function FindAllMarkers or FindMarkers to perform pairwise comparisons to identify marker genes (min.pct = 0.25, logfc.threshold = 0.5). The expression of a signature gene is weighted based on the predicted loss probability calculated from nearest neighbors and the normalized expression summation of all genes in the gene set.

### Statistical analysis

Data are shown as the means ± SEM and representative of at least two independent experiments. Statistical analyses were performed using GraphPad Software. $P$ value was determined by unpaired two-tailed $t$ tests. Statistical analyses of survival curve were compared using a log-rank test. Differences were considered statistically significant if $P < 0.05$.

### Reporting summary

Further information on research design is available in the Nature Portfolio Reporting Summary linked to this article.

## Data availability

Source data are available online for Figs. 1–7 and Supplementary Fig. 1–8. The single cell sequencing data can be obtained from Gene Expression Omnibus (https://www.ncbi.nlm.nih.gov/geo/query/acc.cgi?acc=GSE296919). All other data that support the findings of this study are available from the corresponding author upon request. Source data are provided with this paper.

## Code availability

Our analysis code has been uploaded into the github (https://github.com/huiping400/Fulab_script/tree/main).

## References

1. Philip, M. & Schietinger, A. CD8+ T cell differentiation and dysfunction in cancer. *Nat. Rev. Immunol.* **22**, 209–223 (2021).
2. Chen, L. & Flies, D. B. Molecular mechanisms of T cell co-stimulation and co-inhibition. *Nat. Rev. Immunol.* **13**, 227–242 (2013).
3. Corbet, C. & Feron, O. Tumour acidosis: from the passenger to the driver's seat. *Nat. Rev. Cancer* **17**, 577–593 (2017).
4. Wolf, Y., Anderson, A. C. & Kuchroo, V. K. TIM3 comes of age as an inhibitory receptor. *Nat. Rev. Immunol.* **20**, 173–185 (2020).
5. Sakuishi, K. et al. Targeting Tim-3 and PD-1 pathways to reverse T cell exhaustion and restore anti-tumor immunity. *J. Exp. Med.* **207**, 2187–2194 (2010).
6. Pauken, K. E. & Wherry, E. J. Overcoming T cell exhaustion in infection and cancer. *Trends Immunol.* **36**, 265–276 (2015).
7. Barber, D. L. et al. Restoring function in exhausted CD8 T cells during chronic viral infection. *Nature* **439**, 682–687 (2006).
8. Wherry, E. J. T cell exhaustion. *Nat. Immunol.* **12**, 492–499 (2011).
9. Mo, F. et al. An engineered IL-2 partial agonist promotes CD8(+) T cell stemness. *Nature* **597**, 544–548 (2021).
10. Codarri Deak, L. et al. PD-1-cis IL-2R agonism yields better effectors from stem-like CD8(+) T cells. *Nature* **610**, 161–172 (2022).
11. Zhao, X., Shan, Q. & Xue, H. H. TCF1 in T cell immunity: a broadened frontier. *Nat. Rev. Immunol.* **22**, 147–157 (2021).
12. Sockolosky, J. T. et al. Selective targeting of engineered T cells using orthogonal IL-2 cytokine-receptor complexes. *Science* **359**, 1037 (2018).

13. Aspuria, P. J. et al. An orthogonal IL-2 and IL-2Rβ system drives persistence and activation of CART cells and clearance of bulky lymphoma. Sci. Transl. Med. 13, eabg7565 (2021).
14. Raeber, M. E., Sahin, D. & Boyman, O. Interleukin-2-based therapies in cancer. Sci. Transl. Med. 14, eabo5409 (2022).
15. Hernandez, R., Poder, J., LaPorte, K. M. & Malek, T. R. Engineering IL-2 for immunotherapy of autoimmunity and cancer. *Nat. Rev. Immunol.* **22**, 614–628 (2022).
16. Gaggero, S. et al. IL-2 is inactivated by the acidic pH environment of tumors enabling engineering of a pH-selective mutein. Sci. Immunol. 7, eade5686 (2022).
17. Deryugina, E. I. & Quigley, J. P. Matrix metalloproteinases and tumor metastasis. *Cancer Metast Rev.* **25**, 9–34 (2006).
18. Gobin, E. et al. A pan-cancer perspective of matrix metalloproteases (MMP) gene expression profile and their diagnostic/prognostic potential. BMC Cancer 19, 581 (2019).
19. Blank, C. U. et al. Defining 'T cell exhaustion. *Nat. Rev. Immunol.* **19**, 665–674 (2019).
20. Gyorffy, B. et al. An online survival analysis tool to rapidly assess the effect of 22,277 genes on breast cancer prognosis using microarray data of 1,809 patients. *Breast Cancer Res. Treat.* **123**, 725–731 (2010).
21. Ngiow, S. F. et al. Anti-TIM3 antibody promotes T cell IFN-gamma-mediated antitumor immunity and suppresses established tumors. *Cancer Res.* **71**, 3540–3551 (2011).
22. Ren, Z., Zhang, X. & Fu, Y.-X. Facts and hopes on chimeric cytokine agents for cancer immunotherapy. *Clin. Cancer Res.* **30**, OF1–OF14 (2024).
23. Wang, X. et al. Targeting tumor microenvironment with antibody-guided IL-2 pro-cytokine promotes and rejuvenates dysfunctional CD8 T cells. Signal Transduct. Target. Ther. 8, 268 (2023).
24. Holcomb, E. A. & Zou, W. A forced marriage of IL-2 and PD-1 antibody nurtures tumor-infiltrating T cells. J. Clin. Invest. 132, e156628 (2022).
25. Liu, L. et al. Rejuvenation of tumour-specific T cells through bispecific antibodies targeting PD-L1 on dendritic cells. *Nat. Biomed. Eng.* **5**, 1261–1273 (2021).
26. Xue, D. et al. A tumor-specific pro-IL-12 activates preexisting cytotoxic T cells to control established tumors. Sci. Immunol. 7, eabi6899 (2022).
27. Dixon, K. O. et al. TIM-3 restrains anti-tumour immunity by regulating inflammasome activation. *Nature* **595**, 101–106 (2021).
28. Dixon, K. O., Lahore, G. F. & Kuchroo, V. K. Beyond T cell exhaustion: TIM-3 regulation of myeloid cell. Sci. Immunol. 9, eadf2223 (2024).
29. Alspach, E., Lussier, D. M. & Schreiber, R. D. Interferon gamma and its important roles in promoting and inhibiting spontaneous and therapeutic cancer immunity. Cold Spring Harb. Perspect. Biol. 11, a028480 (2019).
30. Ren, Z. et al. Selective delivery of low-affinity IL-2 to PD-1+ T cells rejuvenates antitumor immunity with reduced toxicity. J. Clin. Invest. 132, e153604 (2022).
31. Zhang, J. H., Huang, D., Saw, P. E. & Song, E. R. Turning cold tumors hot: from molecular mechanisms to clinical applications. *Trends Immunol.* **43**, 523–545 (2022).
32. Lin, K. X. et al. PD-1 and PD-L1 inhibitors in cold colorectal cancer: challenges and strategies. *Cancer Immunol. Immun.* **72**, 3875–3893 (2023).
33. Zhang, T. et al. Up-regulated PLA2G10 in cancer impairs T cell infiltration to dampen immunity. *Sci. Immunol.* **9**, eadh2334 (2024).
34. Shi, W. et al. Next-generation anti-PD-L1/IL-15 immunocytokine elicits superior antitumor immunity in cold tumors with minimal toxicity. *Cell Rep. Med.* **5**, 101531 (2024).
35. Liang, Y. et al. Targeting IFNalpha to tumor by anti-PD-L1 creates feedforward antitumor responses to overcome checkpoint blockade resistance. *Nat. Commun.* **9**, 4586 (2018).
36. Bahmanyar, M. et al. Opportunities and obstacles for the melanoma immunotherapy using T cell and chimeric antigen receptor T (CAR-T) applications: a literature review. *Mol. Biol. Rep.* **49**, 10627–10633 (2022).
37. Wong, K. C. W. et al. Opportunities and challenges in combining immunotherapy and radiotherapy in head and neck cancers. Cancer Treat. Rev. 105, 102361 (2022).
38. Pointer, K. B., Pitroda, S. P. & Weichselbaum, R. R. Radiotherapy and immunotherapy: open questions and future strategies. *Trends Cancer* **8**, 9–20 (2022).
39. Hsu, E. J. et al. A cytokine receptor-masked IL2 prodrug selectively activates tumor-infiltrating lymphocytes for potent antitumor therapy. *Nat. Commun.* **12**, 2768 (2021).
40. Nirschl, C. J. et al. Discovery of a conditionally activated IL-2 that promotes antitumor immunity and induces tumor regression. Cancer Immunol. Res. 10, 581–596 (2022).
41. Curigliano, G. et al. Phase I/Ib clinical trial of sabatolimab, an anti-TIM-3 antibody, alone and in combination with spartalizumab, an anti-PD-1 Antibody, in advanced solid tumors. *Clin. Cancer Res.* **27**, 3620–3629 (2021).
42. de Morais, A. L. G., Cerdá, S. & de Miguel, M. New checkpoint inhibitors on the road: targeting TIM-3 in solid tumors. *Curr. Oncol. Rep.* **24**, 651–658 (2022).
43. Levin, A. M. et al. Exploiting a natural conformational switch to engineer an interleukin-2 'superkine. *Nature* **484**, 529–U159 (2012).
44. Sun, Z. et al. A next-generation tumor-targeting IL-2 preferentially promotes tumor-infiltrating CD8(+) T-cell response and effective tumor control. *Nat. Commun.* **10**, 3874 (2019).
45. Rha, M.-S. & Shin, E.-C. Activation or exhaustion of CD8+ T cells in patients with COVID-19. *Cell. Mol. Immunol.* **18**, 2325–2333 (2021).
46. Suleman, M. et al. Induced inhibition of bovine peripheral blood mononuclear cell proliferation is ameliorated after blocking the immune-inhibitory programmed death 1 receptor. Infect. Immun. 86, e00921–17 (2018).
47. Pilkinton, M. A. et al. Greater activation of peripheral T follicular helper cells following high dose influenza vaccine in older adults forecasts seroconversion. *Vaccine* **35**, 329–336 (2017).
48. Ngwa, W. et al. Using immunotherapy to boost the abscopal effect. *Nat. Rev. Cancer* **18**, 313–322 (2018).
49. Kamphorst, A. O. et al. Proliferation of PD-1+CD8 T cells in peripheral blood after PD-1-targeted therapy in lung cancer patients. *Proc. Natl. Acad. Sci. USA* **114**, 4993–4998 (2017).
50. Khalaf, S. et al. Differential expression of TIM-3 in circulation and tumor microenvironment of colorectal cancer patients. Clin. Immunol. 215, 108429 (2020).
51. Wesolowski, R. et al. Exploratory analysis of immune checkpoint receptor expression by circulating T cells and tumor specimens in patients receiving neo-adjuvant chemotherapy for operable breast cancer. BMC Cancer 20, 445 (2020).
52. Sharma, P. et al. Immune checkpoint therapy-current perspectives and future directions. *Cell* **186**, 1652–1669 (2023).
53. Wang, W. Y. et al. The interaction between lymphoid tissue inducer-like cells and T cells in the mesenteric lymph node restrains intestinal humoral immunity. Cell Reports 32, 107936 (2020).
54. Kovacs, S. B., Oh, C., Aachoui, Y. & Miao, E. A. Evaluating cytokine production by flow cytometry using brefeldin A in mice. *STAR Protoc.* **2**, 100244 (2021).
55. Zheng, G. X. et al. Massively parallel digital transcriptional profiling of single cells. *Nat. Commun.* **8**, 14049 (2017).
56. Hao, Y. H. et al. Integrated analysis of multimodal single-cell data. *Cell* **184**, 3573 (2021).


## Acknowledgements

We are grateful to Li Wu (Tsinghua University, Beijing) for *Zbtb46*-Cre mice; Xiaohuan Guo (Tsinghua University, Beijing) for *Cd4*-Cre mice;

Gencheng Han (Beijing Institute of Basic Medical Sciences, Beijing) for *Lyz2*-Cre and *havcr2* $^{fl/fl}$ mice. We thank Yong Liang, Haitao Jiang, Junfan Chen, Xiaozhe Yin, and Li Yu for providing experiment materials and helpful discussions. We thank the faculties in the animal facility of Tsinghua University. This work was supported by grants from the National Natural Science Foundation of China (82250710684, to Y.F., 32370967 to W.W.) and International Postdoctoral Exchange Fellowship Program (to X. Zhang).

## Author contributions

Conceptualization: X.Z., Y.G., H.L., and Y.-X. F Methodology: X.Z., Y.G., H.L., Z.Y., G.L., and G.H. Investigation: X.Z., Y.G., H.L., Z.Y., W. C., J.W., and W.W. Funding acquisition: X.Z., W.W., and Y-X.F. Supervision: Y-X.F. Writing–original draft: X.Z., Y.G., H.L. Writing–review & editing: X.Z., Y.G., H.L., and Y.-X.F.

## Competing interests

The authors declare no competing interests.

## Additional information

**Supplementary information** The online version contains supplementary material available at https://doi.org/10.1038/s41467-025-60463-4.

**Correspondence** and requests for materials should be addressed to Xuhao Zhang or Yang-Xin Fu.

**Peer review information** *Nature Communications* thanks Ludovic Martinet and the other, anonymous, reviewer(s) for their contribution to the peer review of this work. A peer review file is available.